

Galaxy Zoo: the dependence of morphology and colour on environment^{*}

Steven P. Bamford^{1,2,†}, Robert C. Nichol¹, Ivan K. Baldry³, Kate Land⁴,
Chris J. Lintott⁴, Kevin Schawinski^{4,5,6}, Anže Slosar⁷, Alexander S. Szalay⁸,
Daniel Thomas¹, Mehri Torki¹, Dan Andreescu⁹, Edward M. Edmondson¹,
Christopher J. Miller¹⁰, Phil Murray¹¹, M. Jordan Raddick⁸, Jan Vandenberg⁸

¹*Institute of Cosmology and Gravitation, University of Portsmouth, Mercantile House, Hampshire Terrace, Portsmouth PO1 2EG*

²*Centre for Astronomy & Particle Theory, University of Nottingham, University Park, Nottingham NG7 2RD*

³*Astrophysics Research Institute, Liverpool John Moores University, Twelve Quays House, Egerton Wharf, Birkenhead CH41 1LD*

⁴*Astrophysics, University of Oxford, Denys Wilkinson Building, Keble Road, Oxford OX1 3RH*

⁵*Department of Physics, Yale University, New Haven, CT06511, USA*

⁶*Yale Center for Astronomy and Astrophysics, Yale University, P.O. Box 208121, New Haven, CT 06520, USA*

⁷*Berkeley Center for Cosmo. Physics, Lawrence Berkeley National Lab. & Physics Dept., Univ. of California, Berkeley CA 94720, USA*

⁸*Department of Physics and Astronomy, The Johns Hopkins University, Homewood Campus, Baltimore, MD 21218, USA*

⁹*LinkLab, 4506 Graystone Ave., Bronx, NY 10471, USA*

¹⁰*NOAO Cerro Tololo Inter-American Observatory, 950 North Cherry Avenue, Tucson, AZ 85719, USA*

¹¹*Fingerprint Digital Media, 9 Victoria Close, Newtownards, Co. Down, Northern Ireland, BT23 7GY*

To appear in MNRAS

ABSTRACT

We analyse the relationships between galaxy morphology, colour, environment and stellar mass using data for over 10^5 objects from Galaxy Zoo, the largest sample of visually classified morphologies yet compiled. We conclusively show that colour and morphology fractions are very different functions of environment. Both colour and morphology are sensitive to stellar mass. However, at fixed stellar mass, while colour is also highly sensitive to environment, morphology displays much weaker environmental trends. Only a small part of both the morphology–density and colour–density relations can be attributed to the variation in the stellar mass function with environment.

Galaxies with high stellar masses are mostly red, in all environments and irrespective of their morphology. Low stellar-mass galaxies are mostly blue in low-density environments, but mostly red in high-density environments, again irrespective of their morphology. While galaxies with early-type morphology do always have higher red fractions, this is sub-dominant compared to the dependence of red fraction on stellar mass and environment. The colour–density relation is primarily driven by variations in colour fractions at fixed morphology, in particular the fraction of spiral galaxies that have red colours, and especially at low stellar masses. We demonstrate that our red spirals primarily include galaxies with true spiral morphology, and that they constitute an additional population to the S0 galaxies considered by previous studies. We clearly show there is an environmental dependence for colour beyond that for morphology. The environmental transformation of galaxies from blue to red must occur on significantly shorter timescales than the transformation from spiral to early-type.

We also present many of our results as functions of the distance to the nearest galaxy group. This confirms that the environmental trends we present are not specific to the manner in which environment is quantified, but nevertheless provides plain evidence for an environmental process at work in groups. However, the properties of group members show little dependence on the total mass of the group they inhabit, at least for group masses $\gtrsim 10^{13} M_{\odot}$.

Before using the Galaxy Zoo morphologies to produce the above results, we first quantify a luminosity-, size- and redshift-dependent classification bias that affects this dataset, and probably most other studies of galaxy population morphology. A correction for this bias is derived and applied to produce a sample of galaxies with reliable morphological type likelihoods, on which we base our analysis.

Key words: galaxies: fundamental parameters — galaxies: structure — galaxies: statistics — galaxies: evolution — galaxies: clusters: general

^{*} This publication has been made possible by the participation of more than 100,000 volunteers in the Galaxy Zoo project. Their contributions are acknowledged at <http://www.galaxyzoo.org/Volunteers.aspx>.

[†] E-mail: steven.bamford@nottingham.ac.uk

1 INTRODUCTION

The discovery that galaxies may be naturally classified, simply by their visual appearance, into two principal types: spiral and elliptical, came even before these objects were firmly established as external to our own Galaxy (Hubble 1922). With further study it became clear that the different galaxy types are very differently distributed throughout space (Hubble & Humason 1931). Over the intervening decades our understanding of galaxies has improved dramatically. Nevertheless, explaining the appearance of galaxies, and how this varies with position, remains a central concern.

The visual appearance, or morphology, of a galaxy is an indicator of its current internal structure and kinematics, which in turn are a result of the galaxy's developmental history. Galaxies mainly comprise two structures, a spheroid and a disc. In the most basic terms, elliptical galaxies are simply a spheroid, whereas other morphologies generally comprise a central spheroid along with a larger disc, which often contains spiral arms. These disc and spheroid components appear to develop in very different ways. That the distribution of morphologies changes as a function of position in the universe suggests variability in these developmental processes. This may be the result of cosmological variations, or the interaction of galaxies with their surroundings. Galaxy morphologies therefore offer valuable information with which to construct and constrain theories of galaxy formation and evolution.

The relationships between a galaxy's local environment and its colour and emission line strengths have been particularly well studied recently. Both of these observables are related to star-formation history, and thus physical processes quite different from those that determine a galaxy's morphology. Comparing the behaviour of colour and morphology versus environment may thus provide powerful clues to the mechanisms through which galaxies have developed into the population we see today.

One reason for the current popularity of classifying galaxies by colour and, to a lesser extent, emission line strength, is the ease and accuracy with which these quantities can be measured in modern surveys, such as the Sloan Digital Sky Survey (SDSS). Traditional morphological classification of galaxies, on the other hand, is extremely time consuming - requiring a human visual inspection of each object. Studies have thus far been limited to samples containing several thousand galaxies (Nakamura et al. 2004; Fukugita et al. 2007), although the MOSES project (Morphologically Selected Ellipticals in SDSS; Schawinski et al. 2007) visually inspected nearly 50000 galaxies in order to identify a clean sample of ellipticals.

Attempts at automatic morphological classifications have been made, with varying success. The most common, and arguably most useful, of these are simple measurements which quantify the radial light profile of a galaxy, such as concentration and Sersic index (e.g. Kauffmann et al. 2003; Blanton et al. 2003a). These quantities measure the dominance of a spheroid over any disc component present. However, a spiral galaxy with a bright bulge or nucleus is still a spiral galaxy. Concentration is more strongly related to luminosity than morphology, with more luminous galaxies having more concentrated profiles (Gavazzi et al. 2000). These quantities are therefore not true measures of morphology in the traditional and most discriminating sense (as discussed in the next paragraph). Indeed, van der Wel (2008) finds very different mass and environment dependences for galaxy type-fractions based on concentration versus those derived from an indicator more closely related to visual morphology.

There are several avenues to more sophisticated automatic

morphologies, some which use physical insight or statistical methods to naturally classify galaxies, while others aim to directly reproduce classifications by professional astronomers (e.g. Lahav et al. 1995; Simard et al. 2002; Conselice 2003; Goto et al. 2003; Ball et al. 2004; Allen et al. 2006; Blakeslee et al. 2006; Conselice 2006; Ball et al. 2008; Park et al. 2007). While a number of these approaches are very promising, they do not yet provide a direct equivalent to traditional visual morphology, generally relying instead on the correlations between true morphology and other parameters, such as luminosity, colour and concentration. The human eye has consistently proved better than computational techniques at identifying faint spiral structure in noisy images, the appearance of which is a primary indicator of morphology, along with the relative luminosity of bulge and disk. The presence and form of galaxy spiral arms has important physical implications. These patterns are related to density waves propagating around the disk, and indicate the dynamical state of the galaxy. They are also an important, though not exclusive, mechanism for inducing star formation, and thus provide information on the process by which a galaxy is currently forming its stars. In addition, as the visibility of spiral structures may persist for some time after star formation ceases, their appearance gives an indication of the timescale of any decline in star formation. Finally, to have confidence in any automated technique we must compare with a large number of visually classified objects that cover the full range of galaxy appearance.

The Galaxy Zoo project was born out of the need for reliable, visual morphologies for a large sample of SDSS galaxies. For the reasons mentioned above, the presently available automated methods were deemed insufficient for the task. Our approach was to enlist the public's help to visually morphologically classify all the galaxies in SDSS Data Release 6 (DR6, Adelman-McCarthy et al. 2008) which were targeted for spectroscopy; nearly one million objects. Further details of the Galaxy Zoo project, including its motivation, design and the initial stages of the data reduction, are given in Lintott et al. (2008).

A wide range of science is possible with the Galaxy Zoo dataset. One initial aim of the project, the investigation of a population of rare, blue, star-forming, early-type galaxies, is considered in Schawinski et al. (2008). Another early aim was to measure the statistical properties of spiral galaxy 'spin' orientations, investigated in detail in Land et al. (2008). This present paper makes a start in exploiting the Galaxy Zoo data to study the dependence of morphology on a host of galaxy properties. Here we concentrate on the dependence of morphology on local galaxy environment, how this compares with the dependence of colour on environment, and the role of stellar mass.

1.1 Structure of this paper

Before describing our own study, we set the scene with a brief discussion of previous, related work in Sec. 1.2. Following this, in Sec. 2, we provide details of the data products and sample definitions (2.1), stellar masses (2.2), visual morphologies (2.3) and environmental measures (2.4) that we employ in this paper. Though not essential for understanding our main results, an important component of this work is a quantification of the biases present in the morphological classifications. These are discussed whilst describing our morphologies in Sec. 2.3, but the full details are deferred to Appendix A.

The main results of this paper are presented in Sec. 3 & Sec. 4. Firstly, in Sec. 3, we consider in detail the local relationships between galaxy visual morphology, environment and stellar mass.

Then, in Sec. 4, we compare these morphology relations with those derived using colour to divide the galaxy population, and explore the origins of the differences we find. Our conclusions are summarised in Sec. 5.

1.2 Previous studies of morphology and colour versus environment

The classic papers studying the relationships between visual morphology and environment in the local universe date from the 1980's and early 1990's (Dressler 1980b; Postman & Geller 1984; Whitmore & Gilmore 1991; Whitmore et al. 1993). The study of traditional, visual morphology for large samples of local galaxies has since stood still for the past decade, due to the great effort required to perform such measurements. In contrast, as discussed above, it is now straightforward to measure colours and simple structural parameters for large galaxy samples, and these quantities have therefore taken precedence. It is crucial that we link recent results on large surveys, such as SDSS, back to the wealth of earlier, traditional morphology studies on which much of our understanding is founded.

In order to efficiently sample a wide range of galaxy environments, many studies have concentrated on the regions in and around rich galaxy clusters. In particular, Dressler (1980a) measured the morphology of approximately 6000 galaxies in 55 nearby, rich clusters. Studying this dataset, Dressler (1980b) found a strong relation between local galaxy surface density and morphological type fractions. As local density increases, the spiral fraction was found to fall steadily, the S0 fraction rises in a corresponding manner, and the elliptical fraction increases sharply at the highest densities.

The same dataset was revisited by Postman & Geller (1984), who found that the morphology–density relation extended smoothly to galaxy group environments identified in the CfA redshift survey (Huchra et al. 1983) and by Huchra & Geller (1982) (see Fig. 9). Both Dressler and Postman & Geller identified local density, rather than distance to the centre of the nearest group, as being more closely related to morphology. Whitmore & Gilmore (1991) and Whitmore et al. (1993) again reanalysed the Dressler (1980a) data, but contrastingly claimed that groupcentric distance was a better indicator of morphology than local galaxy density. These opposing results have yet to be resolved. We aim to address this with the Galaxy Zoo dataset in a forthcoming paper.

Studying the dependence of an automated measure of morphology on both local density and groupcentric distance in the SDSS Early Data Release, Goto et al. (2003) found both relations to be strong. Their most striking result is evidence that the fraction of galaxies with intermediate morphological types (early-type spirals, Sa-b) increases with galaxy density before falling at the highest densities. Late-type spirals (Sc-d), on the other hand, steadily decrease in fraction with local density, whereas the elliptical fraction increases sharply at the highest densities. These findings were interpreted as a suggestion that multiple mechanisms were at work in shaping the morphology–density relation.

Many mechanisms have been proposed for the transformation of spiral galaxies to earlier morphological types in dense environments; see Boselli & Gavazzi (2006) for a thorough recent review of the proposed mechanisms and the evidence for them. The mechanisms may be crudely divided into those which simply stop star formation, which indirectly affects morphology by removing the appearance of spiral arms and reducing the prominence of the disk, and those which affect the stellar kinematics of galaxies as well as leading to a cessation of star formation. While both categories of

mechanism can form S0s from spirals, only the latter can create elliptical galaxies.

With the launch of the *Hubble Space Telescope*, studies of morphology versus environment have focused on measuring the evolution with redshift (Smail et al. 1997; Dressler et al. 1997; Poggianti et al. 1999; Treu et al. 2003; Smith et al. 2005; Postman et al. 2005). Trends in morphological fractions versus environment are found at $z \sim 0.5$ –1 that are similar to those measured locally. The principal difference is a reduced fraction of galaxies with S0 morphology in distant intermediate- and high-density cluster environments, balanced by a higher spiral fraction. Neither elliptical galaxies nor the field population show significant evolution. The static nature of the massive elliptical populations has been confirmed by dedicated studies of luminous, red galaxies (LRGs), which find very little evolution in their number density or properties since $z \sim 1$ (Wake et al. 2006).

As mentioned above, environmental trends in galaxy colours and star-formation rates have received much attention recently (Pimblet et al. 2002; Lewis et al. 2002; Gómez et al. 2003; Balogh et al. 2004; Baldry et al. 2004, 2006; Kauffmann et al. 2004; Blanton et al. 2005; Weinmann et al. 2006; Blanton & Berlind 2007). The general result is that the fraction of blue (star-forming) galaxies decreases with local density, in favour of red (passive) objects. Interestingly, the properties of the individual galaxy sub-populations do not appear to change substantially, while their fractions vary greatly. Studies at intermediate redshift find that the fraction of blue, star-forming objects in clusters has decreased substantially since $z \sim 0.5$ –1 (Butcher & Oemler 1984; Dressler & Gunn 1992; Poggianti et al. 1999). This is often associated with the decline of the cluster spiral population (Couch et al. 1998).

The advent of the halo model (Cooray & Sheth 2002) has led to a focus on disentangling the properties of galaxies at the centre of their dark matter halo and satellites orbiting within a larger halo (e.g. van den Bosch et al. 2008). The models frequently assume that all satellite galaxies have ceased forming stars. However, a recent halo-model analysis of the colour-marked correlation function has found that a non-negligible fraction of blue satellites, which depends on satellite mass, is required to reproduce SDSS observations (Skibba 2008). Another interesting finding of such studies is a conformity between the morphologies of satellites and central galaxies (Weinmann et al. 2006; Ann et al. 2008). In this paper we do not attempt to separate central and satellite galaxies, but consider the population as a whole.

Together, all these results suggest that more than one physical process is responsible for the observed dependence of morphology and colour on environment: one which only acts at early times and is responsible for the excess of ellipticals in dense regions, and ongoing processes that prevent further star formation in ellipticals and which transform disc galaxies to early-type morphologies. However, many of the details remain uncertain and speculative. Even so, our current models of galaxy formation are unable to simultaneously reproduce many of the general features of the observational picture.

2 DATA

2.1 Basic galaxy properties

The basis of the data used in this paper is SDSS DR6 (Adelman-McCarthy et al. 2008). For our main analysis we consider only those galaxies in the Main Galaxy Sample, extended

objects with $r_{\text{Petro}} < 17.77$ (Strauss et al. 2002). In addition we only use galaxies with measured spectroscopic redshifts (with $z > 0.01$). Our sample is therefore incomplete in high density environments due to fibre collisions (von der Linden et al. 2007); the spectroscopic completeness in rich clusters is estimated to be $\sim 65\%$ (von der Linden et al. 2007; Yoon et al. 2008). Two SDSS spectrograph fibres cannot be placed closer than 55 arcsec. However, the fibre assignments were based solely on target positions, with no consideration of other galaxy properties, and in cases where multiple targets could only have a single fibre assigned, the target selected to be observed was chosen randomly. Incompleteness due to fibre collisions is therefore independent of galaxy properties. As our analysis considers only trends in the fractions of objects versus environment, rather than absolute numbers, fibre collisions have no significant effect on our analysis. We refer to this sample as our *full sample*; it contains 565798 objects and is used in demonstrating the classification bias in Sec. 2.3 and deriving corrections for it in Appendix A.

We further restrict our main analysis to a redshift range $0.03 < z < 0.085$. We refer to this sample as our *magnitude-limited sample*, containing 192960 objects. The lower redshift limit ensures that the morphological classification bias correction is stable, as explained in Sec. 2.3 and Appendix A. The upper redshift limit is a compromise between the number of galaxies in the sample, the luminosity range over which we are volume-limited ($M_r < -20.17$ mag), and the reliability of the local density estimates.

In order to combine or compare galaxies across a range of redshifts we must account for the redshift dependent selection biases. To remove selection bias from the analyses in this paper we restrict the galaxies considered to those that would meet our apparent magnitude, size and surface brightness criteria if they were located at the upper limit of the redshift range considered. As measures of galaxy size and surface brightness we use the radius containing 50 per cent of the Petrosian flux, R_{50} , and the average surface brightness within this radius, μ_{50} , all from the r -band imaging. Given the upper redshift-limit we adopt, $z < 0.085$, the Main Galaxy Sample limits ($r < 17.77$ mag, $R_{50} \gtrsim 1$ arcsec and $\mu_{50} \lesssim 23.0$ mag arcsec $^{-2}$), and our assumed cosmology (see below), we thus limit to the subsample of *magnitude-limited sample* galaxies with $M_r < -20.17$ mag, $R_{50} > 1.6$ kpc and absolute surface brightness $\mu_{50} < -13.93$ mag kpc $^{-2}$. We refer to this sample, which contains 125923 objects, as our *luminosity-limited sample*. Figure A1 (in Appendix A) shows the redshift distribution for our *luminosity-limited sample*, compared with that of spectroscopically observed objects in the SDSS Main Galaxy Sample. This sample is used for much of the analysis in this paper, with the exception of when we wish to explore down to low stellar masses. In this case we use the *magnitude-limited sample* but either apply a bin-dependent upper redshift-limit to ensure we are complete in each mass-bin, or use a $1/V_{\text{max}}$ weighting. These mass-limited samples are fully defined in the following section.

Our photometry is from the SDSS DR6 UBERCAL (Padmanabhan et al. 2008). Where subscripts are omitted, we use model magnitudes for colours and Petrosian magnitudes otherwise. All magnitudes are on the AB zero-point system and corrected for Galactic extinction. Absolute magnitudes are determined using KCORRECT V4.1_4 (Blanton & Roweis 2007).

Throughout this paper we assume a Friedmann-Lemaître-Robertson-Walker cosmology with $\Omega_m = 0.3$, $\Omega_\Lambda = 0.7$, $H_0 = 70$ km s $^{-1}$ Mpc $^{-1}$.

2.2 Stellar masses

We determine stellar masses from r_{Petro} and $(u-r)_{\text{model}}$ using the relation given in figure 5 of Baldry et al. (2006), which is calibrated on the spectrally-determined stellar masses of Kauffmann et al. (2003) and Glazebrook et al. (2004). Being based on a single colour, these stellar masses may be expected to be of limited accuracy. They display a 0.13 dex scatter around the spectrally-derived masses on which they are calibrated. However, this is comparable to the quoted uncertainties on the spectral measurements (Kauffmann et al. 2003) and the scatter and systematic differences between different spectral mass estimates (Gallazzi et al. 2005). On average, our stellar masses therefore have a comparable accuracy to spectrally-derived estimates. In any case, our colour-based estimates provide a reliable way to rank galaxies, and thus examine trends, with respect to stellar mass.

With the adopted limits of our *luminosity-limited sample*, $z < 0.085$ and $M_r < -20.17$ mag, we become incomplete for red galaxies below a stellar mass of $\sim 10^{10.3} M_\odot$. In order to explore a wider range when binning by stellar mass we must ensure a high level of completeness in each bin. We achieve this, only when considering bins of stellar mass, by lifting the sample absolute magnitude limit, i.e. using the *magnitude-limited sample*, but further limiting the redshift range of objects which contribute to each bin, such that $\lesssim 0.1$ per cent of galaxies in each stellar mass range are omitted due to their being fainter than the survey apparent magnitude limit. For example, in the bin with $\log(\mathcal{M}_*/M_\odot) = 9.9\text{--}10.1$, 99.9 per cent of galaxies are bluer than $(u-r) = 2.96$, and hence have $\log(\mathcal{M}_*/L_r) < 0.37$ in solar units (from the calibration of Baldry et al. 2006). For $\log \mathcal{M}_*/M_\odot = 9.9$ this corresponds to an absolute magnitude limit of $M_r < -19.18$. The survey apparent magnitude limit of $r < 17.77$ and assumed cosmology thus require that we restrict objects in this stellar mass bin to $z < 0.055$. We also ensure completeness in terms of size and surface-brightness in the same manner as for the *luminosity-limited sample*, by limiting these quantities to the range of values observable at the highest redshift considered, $z < 0.085$. Given the low redshift limit of our *magnitude-limited sample*, $z \geq 0.03$, we are able to study galaxies with stellar masses down to $\log \mathcal{M}_*/M_\odot = 9.5$ in statistically useful numbers. We refer to this as our *binned mass-limited sample*.

Occasionally we will wish to produce a relation for a sample which is complete down to a low stellar mass limit, but for which limiting the redshift range as described above would leave us with too few high-mass galaxies. In this case we use the *magnitude-limited sample*, but weight each object by $1/V_{\text{max}}$, where V_{max} is the volume in which it would have been possible to observe that object given its absolute magnitude, size, and surface brightness, and given the survey limits on the corresponding apparent quantities. With this weighting we can limit to $\log \mathcal{M}_*/M_\odot > 9.8$ without excessive uncertainty, and refer to this as our *V_{max} -weighted mass-limited sample*.

2.3 Galaxy Zoo morphologies

The morphologies utilised in this paper are derived from classifications by over 80,000 members of the international public as part of the Galaxy Zoo project. This project is described in detail by Lintott et al. (2008). Briefly, each galaxy received several, independent morphological classifications, each by a different user. The four possible classifications were labelled as: ‘elliptical’, ‘spiral’, ‘don’t know’, and ‘merger’. The ‘elliptical’ class, in addition to containing galaxies with elliptical morphology, also contains the

majority of S0 galaxies, as will be shown later in this section. We therefore refer to it henceforth as the early-type class. The merger class is mainly comprised of interacting pairs, generally with tidal features, which may or may not be expected to eventually merge. It also suffers from some degree of contamination from galaxy pairs that are overlapping in projection, but not physically related. This is of no consequence to the present paper, however, as only a small fraction (< 1 per cent) of objects are identified as a merger by a majority of classifiers, and these classifications are not specifically considered further herein. The spiral classification was subdivided into ‘clockwise’, ‘anti-clockwise’, and ‘edge-on/unsure’, referring to the direction and orientation of the spiral arms. This was primarily for use in studies of galaxy spins (Land et al. 2008; Slosar et al. 2008). However, it also provides us with an indication of whether a galaxy was classified as spiral due to either noticeable spiral structure or a disk, edge-on appearance.

The median number of classifications per object is 34, with 98 per cent of our *full sample* having at least 20 classifications each. These classifications were processed into raw ‘likelihoods’ for a galaxy being of a given morphological type, directly from the proportion of classifications for each type. We denote these as p_{el} , p_{sp} , p_{dk} and p_{mg} for early-types, spirals, ‘don’t know’ and mergers, respectively.

A choice that must be made is how to go from the measured morphological-type ‘likelihoods’ to individual morphologies and type fractions. This choice depends upon the intended usage of the data. If one requires reliable morphologies for individual galaxies, or samples containing just one type, then assigning classifications to galaxies with type likelihoods above a certain threshold is appropriate. The downside of this is that it results in a significant fraction of the sample being unclassified, these being objects with a spread of likelihood between two or more types. The choice of threshold is somewhat arbitrary, depending on the ‘cleanness’ and size of the required sample. The characteristics of samples defined using Galaxy Zoo thresholded classifications are considered in more detail by Lintott et al. (2008).

Alternatively, if one is interested in type fractions, then the likelihoods themselves can be used in the statistics. This retains more information than thresholding, and all galaxies can be included, but it cannot provide classifications for individual objects. Figure 1 shows the Galaxy Zoo type fractions as a function of redshift, determined by both thresholding ($p > 0.8$) and directly using the raw measured likelihoods. Assuming that there is negligible evolution in the galaxy population over the redshift interval considered, and that the survey contains a similar distribution of environments at each redshift, then the true type fractions should be constant with redshift. As these two assumptions are expected to be reliable, any trends in the observed GZ type fractions with redshift may be attributed to a combination of two biases. The first is selection bias, due to variation in the size and luminosity distribution of galaxies in our *magnitude-limited sample*, resulting from the apparent selection limits. The second is classification bias, the tendency for otherwise identical galaxies viewed at different distances to receive different morphological type classifications, due to signal-to-noise and resolution effects.

Figure 1 also illustrates the difference in type fractions when weighted or unweighted type likelihoods are used (see Lintott et al. 2008). The effect of the weighting is to further increase the apparent fraction of early-type galaxies with increasing redshift. However, the effect is small and only significant when thresholded classifications are used. Throughout the rest of this paper we use the unweighted type likelihoods, without thresholding.

As trends are clearly present in Fig. 1, the raw type likelihoods are, in general, biased. In Fig. 2 we attempt to remove selection effects below given redshifts by limiting in absolute magnitude. The thin lines in this figure correspond to the raw type likelihoods. They still show strong trends with redshift, indicating that classification bias is present in the raw Galaxy Zoo data.

For otherwise morphologically-identical galaxies, apparently fainter and smaller objects are more likely to be classified as early-type due to the diminished spatial resolution and signal-to-noise. However, this classification bias can be statistically corrected for, by applying an adjustment to the raw type likelihoods. These adjusted likelihoods, $p_{\text{el,adj}}$ and $p_{\text{sp,adj}}$, may then be used to generate type fractions that are unbiased with respect to galaxy luminosity, size and redshift. The thresholding approach may also be based on these de-biased likelihoods, or limited to considering galaxies in regions of parameter space where the biases are shown to be small. The classification bias and our procedure for removing it are explained in detail in Appendix A. For the remainder of this paper the type fractions we consider are estimated by averaging the de-biased type likelihoods over bins of galaxy parameter space.

The performance of our de-biasing procedure may be judged from the thick lines in Fig. 2. These indicate the type fractions after application of the de-biasing procedure. In the redshift range that is free from selection effects the de-biased type fractions are approximately flat and, in particular, the ratio of early-types to spirals is constant. This indicates that the de-biasing procedure is working as anticipated. The downturn in early-type fraction at low redshift for the sample with the fainter limit is likely due to two effects. The small volume at low redshifts leads to a reduced occurrence of bright, and hence preferentially early-type, objects. In addition, the de-biasing procedure relies on the lowest redshift bins to establish a baseline luminosity–size distribution against which higher redshifts are compared. Therefore, the lowest redshift bins cannot be entirely corrected by the procedure we adopt. To avoid this issue with our bias correction we limit our main analysis samples to $z \geq 0.03$. This conservative cut reduces the number of objects in our *luminosity-limited sample* by only 3 per cent.

To give an impression of the how the galaxy images translate into morphological-type ‘likelihoods’, Fig. 3 shows examples for $p_{\text{sp}} \sim (0.1, 0.5, 0.9)$ for four different luminosity–size bins at fixed redshift. One can see that the appearance of spiral or disk features become clearer with increasing p_{sp} .

Finally, we highlight that S0 galaxies are not considered as a separate class in this work, due to the difficulty in discriminating them from the other classes and our initially conservative expectations of the abilities of our classifiers. Face-on S0s are difficult to distinguish from elliptical galaxies, whilst edge-on S0s may appear the same as edge-on spirals. Even those who are highly experienced in morphological classification struggle with these distinctions.

The Galaxy Zoo classification scheme specifies that objects with visible spiral arms or an edge-on appearance should be classified as spirals, the remainder should generally be assigned to the early-type classification. The ‘don’t know’ option is available for those who decide the image quality is insufficient for them to make the distinction, or for objects that do not appear to be galaxies. However, this resort was rarely chosen, partly because the Galaxy Zoo interface does not explicitly indicate the image resolution, and under-resolved galaxies of any type often appear to have elliptical morphology. Face-on or moderately inclined S0s will thus be found in the Galaxy Zoo early-type class. We can test this by examining the Galaxy Zoo type-likelihood distributions for objects classified by experts. For this we use the largest sample of

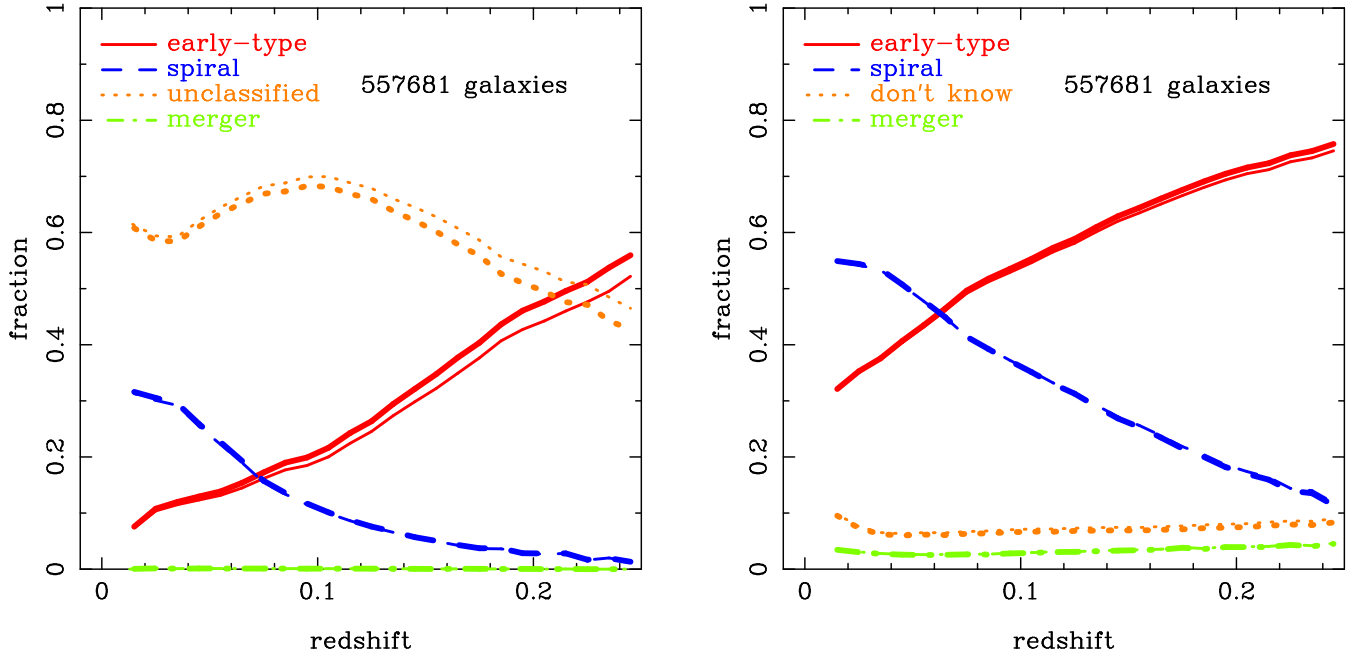


Figure 1. Morphological type fractions from our *full sample* of raw Galaxy Zoo likelihoods, plotted as a function of redshift. Classifications are based (left) on a likelihood threshold of $p > 0.8$, and (right) directly on the likelihoods themselves. The thick and thin lines corresponds to the weighted and unweighted likelihoods, respectively. “Unclassified” refers to all objects which do not meet the threshold of $p > 0.8$ for any class, whereas “don’t know” refers to the likelihood of an object belonging to the “don’t know” class, i.e. the fraction of times the classifiers clicked the “don’t know” button.

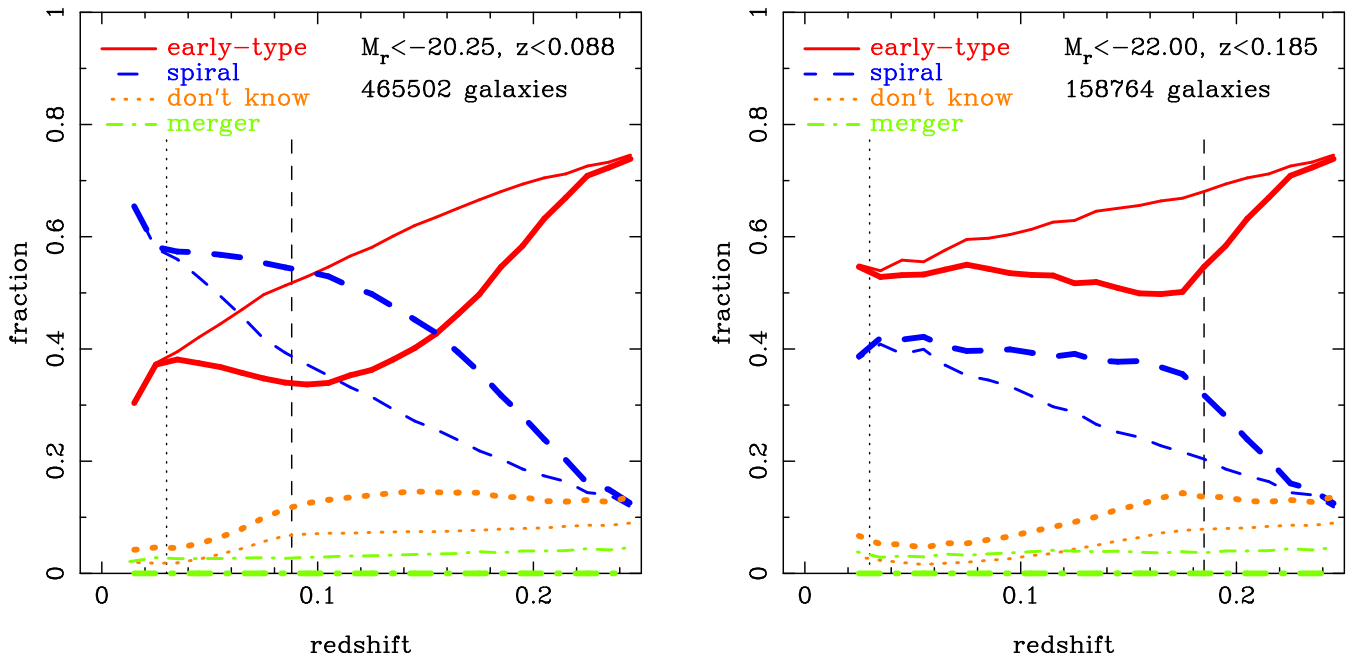


Figure 2. Morphological type fractions, from our *full sample* of unweighted Galaxy Zoo likelihoods, as a function of redshift. The thick and thin lines correspond to the de-biased and raw likelihoods, respectively. Selection effects have been removed below (left) $z = 0.088$ and (right) $z = 0.185$ by imposing the magnitude limits given in each panel. These redshifts are indicated by the vertical dashed lines. The vertical dotted line in each panel indicates the low redshift limit ($z \geq 0.03$) applied to all our main analysis samples. Note that the ratio of de-biased early-type and spiral fractions is roughly constant over the redshift range for which selection effects are not present.



Figure 3. Example images illustrating the appearance of galaxies with different morphological-type likelihoods. Objects in the left, centre and right columns have $p_{\text{sp}} \sim 0.1, 0.5$ and 0.9 , respectively. All objects are at a redshift $z \sim 0.05$, but each row corresponds to a different luminosity–size bin, from top to bottom: $(M_r, R_{50}) = (-22.625, 7.75), (-22.375, 5.75), (-21.875, 4.25), (-20.375, 2.25)$, corresponding to the white dots in Fig. A6. These bins lie in the transition region between early-types and spirals in luminosity–size space, and are therefore not representative of our general sample, but provide a convenient comparison of otherwise similar objects with different morphological-type likelihoods. Each image is scaled to $10R_{50}$ on a side.

morphologically-classified SDSS galaxies that attempts to distinguish S0s from the other types, provided by Fukugita et al. (2007, hereafter F07). The early-type and spiral type-likelihood distributions are shown in Fig. 4 (this reproduces Fig. 8 from Lintott et al. (2008) with the addition of histograms showing the de-biased type likelihoods used in this paper). We show distributions for the F07 ellipticals, spirals, and S0s, as well as ambiguous objects that are classified as E/S0 or S0/Sa.

The majority of objects that F07 classify as E/S0 or S0 have high p_{el} and low p_{sp} (both raw and de-biased). The S0/Sa galaxies span a range of intermediate p_{el} and p_{sp} . We might expect edge-on S0s to be assigned to the spiral class in Galaxy Zoo. However, Fig. 4 shows that extremely few of the F07 E/S0, S0 or S0/Sa galaxies receive high p_{sp} . For the F07 sample, despite there being one S0 for every four spirals, S0s contribute just 3 percent to the Galaxy Zoo spiral fraction. Either edge-on S0s identified by F07 appear more like ellipticals than spirals to the Galaxy Zoo classifiers, or F07 and Galaxy Zoo both classify edge-on S0s as spirals, or perhaps a combination of the two. Lintott et al. (2008) demonstrate that this is also true when thresholded classifications based on the raw type likelihoods are used. In any case, the uncertain distribution of true S0s between the classes henceforth referred to ‘early-type’

and ‘spiral’ should be borne in mind when considering the results of this paper.

2.4 Measuring environment

2.4.1 Local galaxy density

We estimate local galaxy density by following exactly the detailed prescription in Baldry et al. (2006), but extended from DR4 to DR6. The local density for a galaxy is given by $\Sigma_N = N/(\pi d_N^2)$ where d_N is the projected distance to the N th nearest neighbour that is more luminous than $M_r = -20$ (with a small evolution correction, see below). In our analysis we use an estimate of local galaxy density, Σ , determined by averaging $\log \Sigma_N$ for $N = 4$ and 5 . In addition, the area πd_N^2 is modified close to a photometric edge; and Σ is determined by averaging the density determined using spectroscopic neighbours ($|c \Delta z| < 1000 \text{ km s}^{-1}$) with that determined using both spectroscopic and photometric neighbours ($|\Delta z| < z_{\text{err},95}$, the 95 per cent confidence interval, for galaxies with only photometric redshifts determined by Baldry et al. 2006). The highly continuous imaging coverage in DR6 thus increases the number of galaxies with accurate local density estimates significantly beyond that expected simply from the increase in area since DR4.

The *density defining population* is constructed independently of the other samples used in this paper. It comprises all galaxies with $r < 18$ in DR6 and with $M_r < M_{r,\text{limit}} - Q(z - z_0)$, where $M_{r,\text{limit}} = -20$ and $Q = 1.6, z_0 = 0.05$ account for evolution as determined by Blanton et al. (2003b). With these parameters, local density measurements are reliable for $z < 0.085$, the redshift to which the density defining sample is luminosity-limited. For density defining galaxies without spectroscopic redshifts, M_r is determined using the redshift of the galaxy whose environment is being measured. We determine the potential range in $\log \Sigma$ that may result from both edge effects and the use of galaxies with only photometric redshifts. Galaxies for which the full range of potential $\log \Sigma$ is larger than 0.75 dex are rejected from the analysis sample. This amounts to ~ 10 per cent of objects, reducing our *luminosity-limited sample* to 113579 objects when we are considering local density. This sample has a $\log \Sigma$ uncertainty range of less than 0.4 and 0.15 for 75 and 50 per cent of galaxies, respectively. For 25 per cent of our *luminosity-limited sample* the density is based on only spectroscopic galaxies far from survey edges, and thus the uncertainty range attributable to these issues is zero.

As noted by van der Wel et al. (2007) it may be more meaningful to limit the density-defining population in terms of stellar mass, rather than luminosity. However, as van der Wel et al. show, while this may change the absolute values and distribution of local density, it does not significantly affect the ranking of galaxy environments, and thus would have no effect on our conclusions.

2.4.2 Group properties

In the standard Λ CDM cosmology, the properties of galaxies are thought to have a strong dependence on the characteristics of the dark matter halo in which they reside (Cooray & Sheth 2002). Even without assuming this background model, the empirical clustering of galaxies into groups suggests a natural scale on which to measure environment. The local density around a galaxy, as measured by the distance to its fifth-nearest neighbour, may fluctuate significantly and rapidly compared with the timescales for galaxy evolution. Therefore, recent environmental influences on the properties

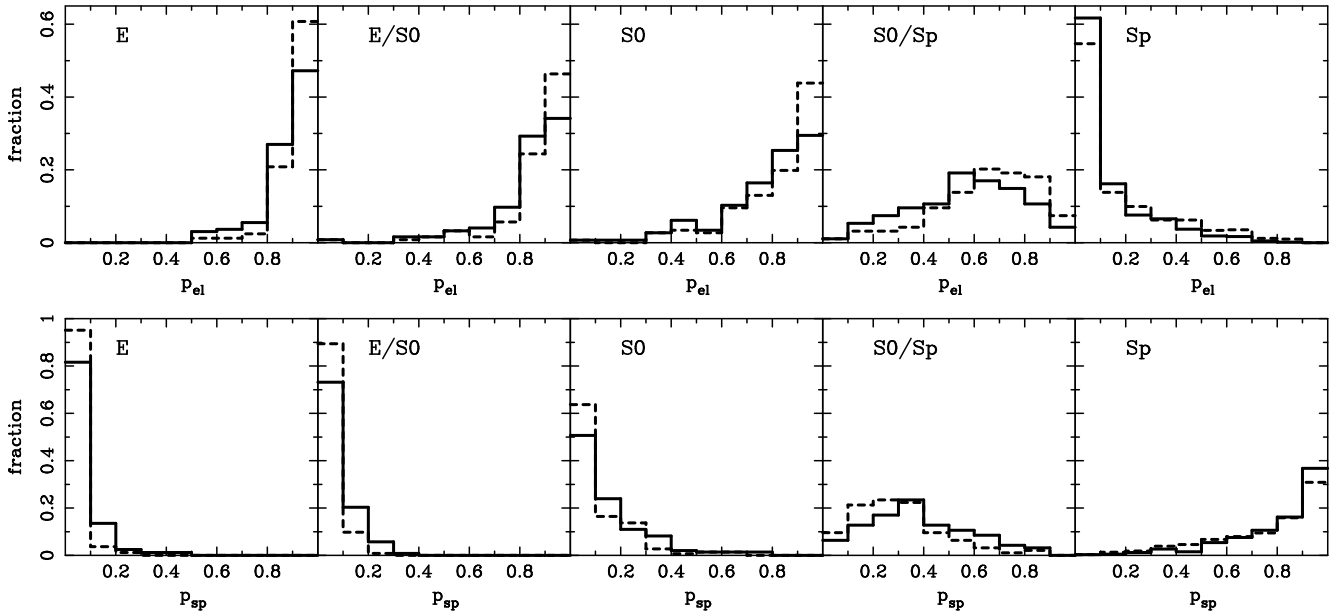


Figure 4. Distribution of (top) early-type and (bottom) spiral morphological type likelihoods for galaxies in our *luminosity-limited sample* with classifications from Fukugita et al. (2007, F07). Each panel contains objects classified by F07 as having the indicated morphological type. The dashed and solid lines correspond to the raw and de-biased type likelihoods, respectively.

of a galaxy may not be reflected by the local density measured for that galaxy now. On the scale of galaxy groups, changes in environment will generally be slower and smoother. It is unclear, however, which environmental scales play a significant role. Determining this is complicated by strong correlations between different environmental measures.

To probe the influence of galaxy groups we utilise the C4 catalogue of galaxy groups and clusters (Miller et al. 2005). The C4 catalogue was constructed by identifying galaxy overdensities simultaneously in both three-dimensional position and four-dimensional colour-space. This method greatly reduces the twin problems of projection effects and redshift-space distortions in identifying physical galaxy groups. Tests indicate that the C4 catalogue is ~ 90 per cent complete and ~ 95 per cent pure above $\mathcal{M}_{C4} = 10^{14} h^{-1} \mathcal{M}_{\odot}$ and within the redshift range considered here (Miller et al. 2005). The method for estimating the virial radius, and hence virial mass, for the C4 groups has been refined beyond those given in the original catalogue (Torki et al. 2008).

At the time of analysis the C4 catalogue was only available for DR5. Whenever considering group quantities we thus limit our sample to objects with spectroscopy in DR5, though we continue to use DR6 measurements. We will employ two estimates of environment based on the C4 groups: the distance from a galaxy to its nearest C4 group, and the mass of the nearest C4 group.

In order to determine the distance from a galaxy to its nearest group we require both the line-of-sight and projected distances between them. A first approach is to convert redshifts, via an assumed cosmology, directly to line-of-sight distances between the galaxies and their nearest C4 group, d_{C4} . However, this neglects the peculiar motions of galaxies. These motions are small for isolated galaxies, but increase in denser regions. They comprise two effects. First, there is a coherent infall in the vicinity of groups (Kaiser 1987), but the velocities associated with this are generally low and produce a fairly small effect on the inferred galaxy distances. Secondly, there are the random motions of virialised group members. These virial motions are significant compared with cosmological velocities, par-

ticularly at low redshift. The effect is such that galaxies which are truly group members are inferred to be at very different line-of-sight distances: the ‘Fingers of God’ effect. To correct for this one must identify galaxies that are likely to be group members, and put them at the same line-of-sight distance as their parent group. Our procedure for doing this is detailed in Appendix B, resulting in corrected distances, D_{C4} , which are additionally normalised by the virial radius of the nearest C4 group.

When using groupcentric distances, we limit the galaxies considered to those which are closer to a C4 group than they are to an edge of the DR5 spectroscopic survey region. We also permit a galaxy’s nearest C4 group to lie beyond the redshift limits of our *magnitude-limited sample*. We thus avoid the issue of clusters possibly located just beyond the survey and sample boundaries. Recall that our redshift limits are $0.03 < z < 0.085$, and so our *magnitude-limited sample* is restricted to redshifts where the C4 group catalogue is reasonably complete (~ 90 per cent: Miller et al. 2005).

Although they measure different quantities, the environmental measures based on groups correlate strongly with local density. Figure 5 shows the relationship between local galaxy density and our two measures of distance from a C4 group. At large distances from a C4 group ($\gtrsim 10$ Mpc or R_{vir}) galaxies are found in the full range of local densities, although predominantly these densities are low. However, approaching a C4 group the minimum local density steadily increases, such that all galaxies in the vicinity of C4 groups are also in regions of high local density.

Correcting for the ‘Fingers of God’ effect clearly improves the correlation between distance to a C4 group and local density. There remain a large number of objects in regions of fairly high local density which are distant from a C4 group. There are several potential reasons for this: (i) even though density and group distance may be strongly related, the C4 catalogue forms an incomplete census of galaxy groups; (ii) the ‘Fingers of God’ suppression is not fully effective, it has a reduced efficiency for objects at intermediate densities – for which we cannot distinguish between true

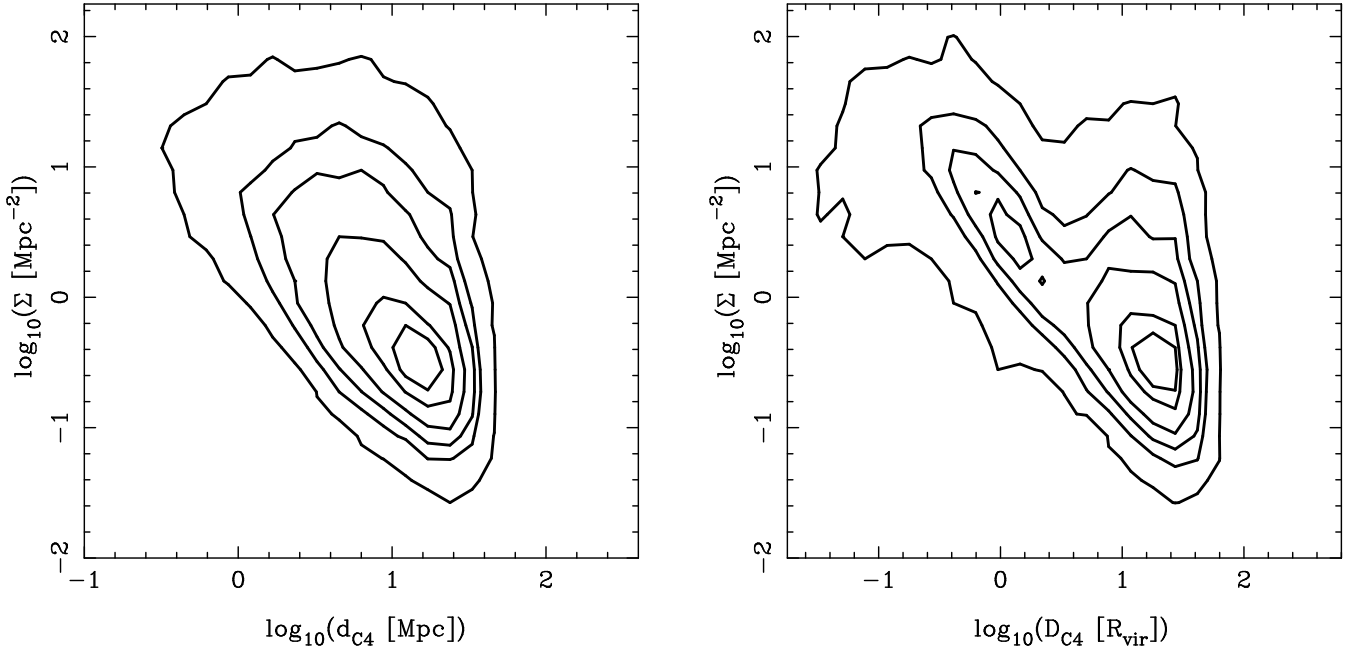


Figure 5. Local galaxy density versus (left) raw and (right) corrected distance to the nearest C4 group. Contours enclose 10, 25, 50, 75, 90 and 99 per cent of galaxies in the *luminosity-limited sample*.

group members and nearby, but gravitationally unbound, objects – and is designed to be conservative and under-correct in such circumstances, preferring incompleteness over contamination of the group members sample; (iii) the redshift interval over which local density is measured is large enough to allow nearby groups to influence the local density estimate for some isolated objects, but note that we do limit the local density uncertainty, see Sec. 2.4.1; (iv) high local densities may occur in structures which do not meet the requirements to be selected as C4 groups, e.g. filaments, too few members, inhomogeneous member colours, etc. All of these issues are likely together responsible for the spread in local density at large distances from C4 groups and the bimodality visible along the line of (anti-)correlation between density and group distance.

Close to C4 groups, within a few Mpc or virial radii, we expect a spread in local density due to substructure – azimuthal variations in local density. Even so, local density is confined to higher values than seen in the more typical environments. For substructures containing more than five density-defining galaxies the local density estimate will be well localised on the sky. However, low density measurements around groups may be precluded by the method’s limited line-of-sight resolution. Nevertheless, the overall correlation between local density and C4 group distance must be a real effect.

Local galaxy density and distance to a C4 group are thus useful alternative estimates of environment, with different caveats for their interpretation. The agreement of results when using either of these methods will therefore be a good sign that the results are robust with respect to the general concept of ‘environment’. Any contrasts in the results from these two methods may point to different effects at work in classical groups and in more general dense regions.

For galaxies within the influence of a C4 group, the mass of that group may well be expected to determine the magnitude of any environmental effect. The local density for members of C4 groups is shown in the left panel of Fig. 6 as a function of C4 group mass. As Fig. 5 suggests, galaxies within the virial radius of C4 groups are

confined to high local galaxy densities. This is clearly seen by comparing the histograms for cluster members and all galaxies along the side of the left panel in Fig. 6. However, there is almost no trend in the distribution of local galaxy density versus the mass of the group.

The right panel of Fig. 6 shows the same plot as the left, but now containing all galaxies within a fixed physical radius, 3 Mpc, of a C4 group. A trend with group mass is now much more apparent. Comparing the left and right panels of Fig. 6 illustrates that the primary role of group mass is in determining the scale of the region, through the virial radius, over which local galaxy density is elevated, rather than the determining the absolute degree of density enhancement.

3 MORPHOLOGY VERSUS ENVIRONMENT

3.1 Local galaxy density

As a first look at the Galaxy Zoo morphology–density relation, and a final demonstration of the removal of classification bias, in the left panel of Fig. 7 we plot the early-type fraction based directly on the raw type likelihoods, as a function of local galaxy density. This is shown for objects in four redshift slices. Note the offsets between the redshift slices: the average raw early-type fraction increases with increasing redshift, due to classification bias. However, in each redshift bin a clear relation can be seen, with early-type galaxies favouring higher density environments.

To produce a single, reliable, local morphology–density relation we use the de-biased type likelihoods described in Sec. 2.3 and derived in Appendix A. The resulting morphology–density relations are shown in the right panel of Fig. 7 for the same four redshift slices as the left panel. Clearly the de-biasing procedure works well, as the relations from independent redshift ranges now match. We can thus combine galaxies over the full redshift range we are considering, $0.03 < z < 0.085$. The morphology–density

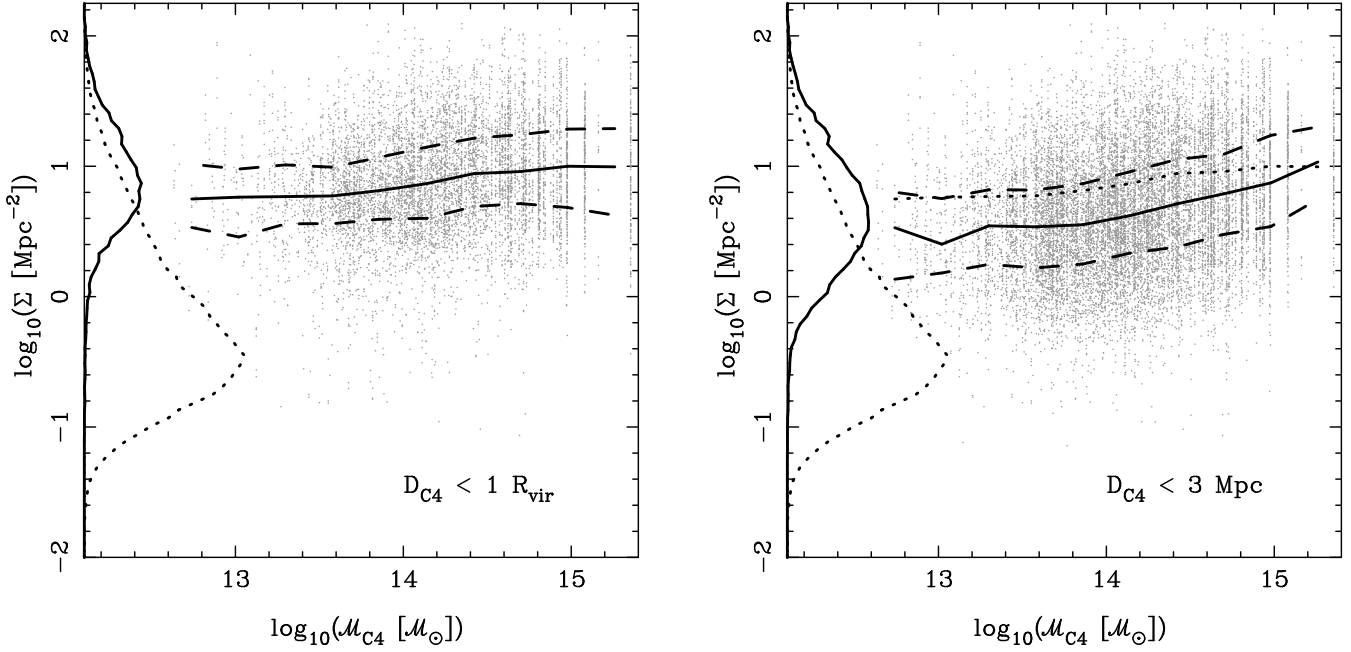


Figure 6. (Left) points indicate local galaxy density versus C4 group mass for members of C4 groups with $D_{C4} < 1 R_{\text{vir}}$. The solid and dashed lines through the points indicate the median and quartiles of $\log \Sigma$ in bins of \mathcal{M}_{C4} . Along the left-hand side of the plot appear histograms comparing the $\log \Sigma$ distribution for C4 group members (solid) with that for all galaxies (dashed). The frequencies for the histogram of C4 group members have been multiplied by four to improve visibility. (Right) as the left panel, but now for objects within a constant 3 Mpc radius of each C4 group ($D_{C4} < 3 \text{ Mpc}$). The additional dotted line indicates the median relation from the left panel.

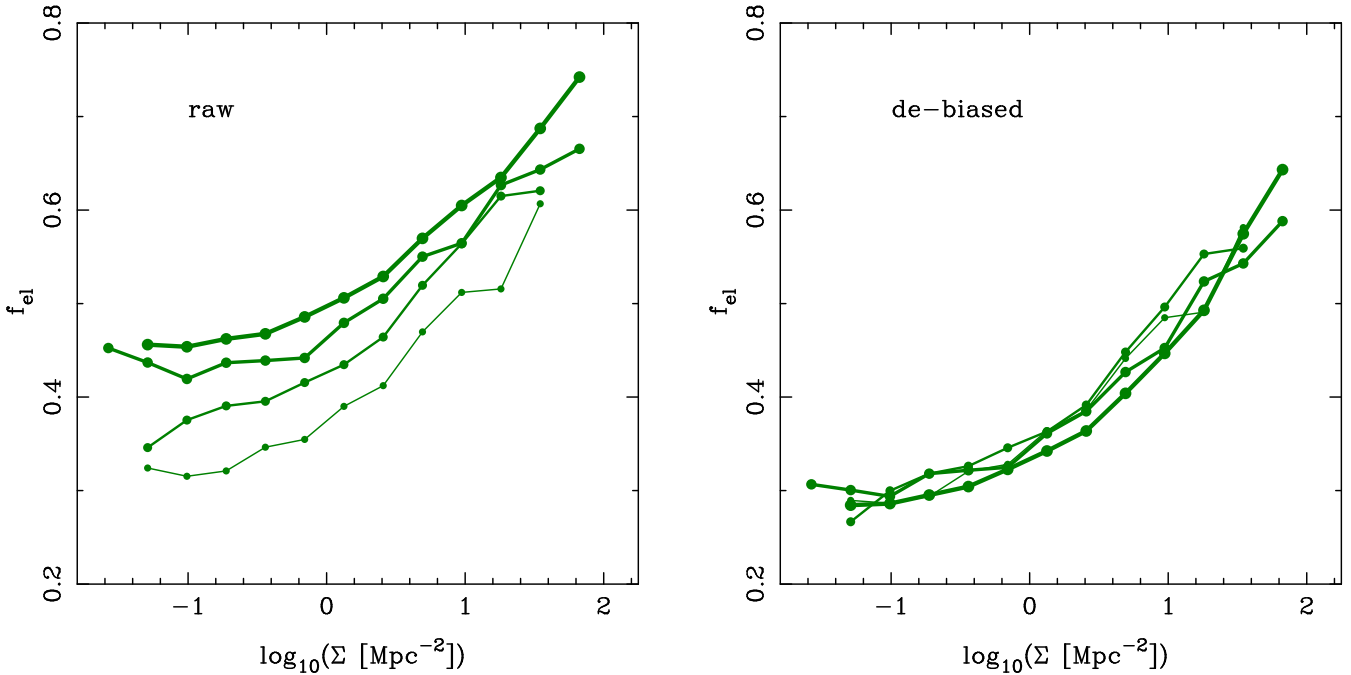


Figure 7. Early-type fraction versus local galaxy density for four redshift bins ($z \sim 0.037, 0.051, 0.064, 0.078$). The left and right panels show the fractions determined from the raw and de-biased morphological type likelihoods, respectively.

relation for our full *luminosity-limited sample*, containing information on 113579 galaxies, is shown in Fig. 8. We determine the uncertainties on the mean type fraction in each bin from the standard deviation of the type likelihoods divided by the square-root of the number of objects in each bin. The reliability of these uncertainties has been confirmed by bootstrap resampling. In all plots we show

2σ uncertainty ranges. (The colour–density relation is also shown in Fig. 8 and subsequent figures, for which red galaxies are defined as those on the red side of the $u - r$ versus stellar mass bimodality using the divider determined by Baldry et al. (2006). However, we defer discussion of this relation until Sec. 4.)

Our morphology–density relation is extremely well defined.

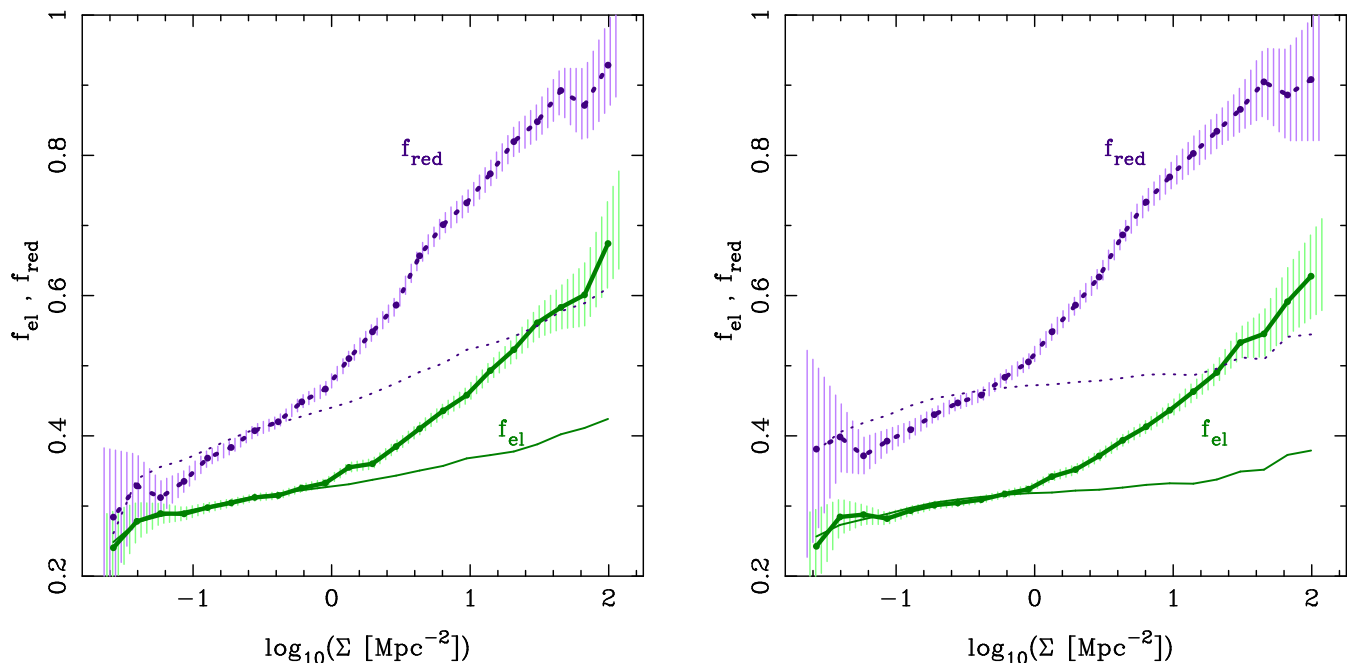


Figure 8. Early-type (green, thick, solid line) and red (purple, thick, dotted line) fractions versus local galaxy density for galaxies in (left) our *luminosity-limited sample* and (right) our V_{\max} -weighted mass-limited sample, complete for stellar masses $\log(\mathcal{M}_*/\mathcal{M}_\odot) > 9.8$, and constructed by applying $1/V_{\max}$ weightings to our *magnitude-limited sample* (see Sec. 2.2). The early-type fraction is determined from the de-biased type likelihoods, as described in Sec. 2.3. The shaded regions indicate the 2-sigma statistical uncertainties on each equally-spaced $\log \Sigma$ bin. Thin lines show the contribution to each relation attributable to variation in the stellar mass function with environment (see Sec. 3.1.1). The early-type fraction is discussed alone in Sec. 3, and compared with the red fraction in Sec. 4.

It is consistent with a monotonic function, with a significant gradient over almost the whole range of galaxy densities that occur, $0.1 \lesssim \Sigma \lesssim 25$ galaxies Mpc^{-2} . Even outside this range, there is no evidence for the relation flattening off completely. While more complicated representations could be acceptable, the data suggests that the relation is most appropriately described by a single, smooth function.

To compare our morphology–density relation to previous studies, in Fig. 9 we reproduce the relations from Postman & Geller (1984, hereafter PG84), which contains a combination of data for galaxies in clusters, from Dressler (1980a), and groups, from the CfA redshift survey (Huchra et al. 1983) and Huchra & Geller (1982). In PG84 the local density is measured in a rather different manner to that employed in this paper. However, to qualitatively compare our relation to these classic results we attempt to convert our measured local surface densities (Σ) to the local volume density scale (ρ) of PG84. We correct for the different depths of the density defining populations ($M_B < -17.5$ versus $M_r \lesssim -20.0$) by empirically determining the number density ratio given these selection limits, as a function of local surface density. We convert from surface to volume densities assuming the overdensity to be spherical. Finally we adjust to $H_0 = 100 \text{ km s}^{-1} \text{ Mpc}^{-1}$. The resulting relation is shown by the thick green line in Fig. 9.

As discussed in Sec. 2.3, S0 galaxies are not explicitly separated from the other types in the Galaxy Zoo data. However, the trend in the combined PG84 elliptical + S0 fraction with local density is very similar to our relation. A comparison of the type fractions suggests that the Galaxy Zoo early-type class contains the majority of the S0 population, as also indicated by our earlier comparison with F07 in Fig. 4. We defer the separation of the elliptical and S0 populations to a future Galaxy Zoo project.

The remaining differences between our early-type fraction

versus local density relation and that of PG84 may be attributed to a number of issues, but the most important is the differing selection functions of the Galaxy Zoo and PG84 samples. As shall shortly be demonstrated, the morphology–density relation is strongly dependent upon the stellar mass (or luminosity) of the galaxies considered, and thus different sample selections will naturally produce different relations.

3.1.1 Stellar mass dependence

A significant advantage of the Galaxy Zoo sample, in comparison with previous visual morphology catalogues, is its size. It is possible to subdivide our sample in terms of various properties, and still retain sufficient galaxies in each subsample to make reliable inferences. In particular, we can consider morphology trends in narrow bins of stellar mass.

It is now well known that the stellar mass function of galaxies varies with environment (Balogh et al. 2001; Zehavi et al. 2002). This can be, to some extent, theoretically understood by the biasing of the dark matter halo mass function varying with the large-scale density field (Sheth & Tormen 1999; Mo & White 2002; Mo et al. 2004; Skibba et al. 2006), although there are still many unsolved issues in connecting haloes with galaxies. In the left panel of Fig. 10 we show how the distribution of stellar mass depends on local galaxy density in our *luminosity-limited sample*. The distribution of stellar masses steadily shifts to higher masses with increasing local density.

The mass function of galaxies is also expected to depend on morphological type (Maller 2008), as it varies with other galaxy properties (Croton et al. 2005; Baldry et al. 2006). We shall see this clearly later in this section. In dense large-scale environments we expect a greater fraction of high-mass haloes, and such haloes

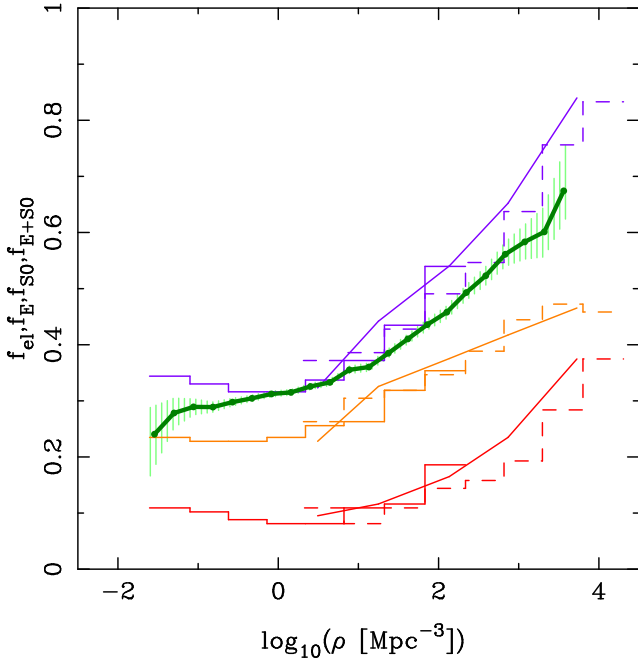


Figure 9. The thin lines reproduce the morphological type fractions versus local galaxy volume density from figure 1 of Postman & Geller (1984). From low to high, the groups of lines correspond to ellipticals (red), S0 galaxies (orange), and ellipticals and S0 galaxies combined (purple). In each group, the solid and dashed histograms represent data from CfA groups and clusters, respectively (Huchra et al. 1983), and the line indicates the converted cluster relation of Dressler (1980a). For comparison, the points joined by a thick green line show the Galaxy Zoo early-type fraction versus local surface density relation from Fig. 8 converted to the volume density scale of Postman & Geller (1984), as described in the text.

are preferentially inhabited by galaxies with high stellar mass and early-type morphology. We must therefore consider whether the observed morphology–density relation may simply be a consequence of these effects.

One way we can test this is by determining the morphology–density relation that would be present in our sample on the assumption that the early-type fraction is only a function of stellar mass. To do so, we directly measure the dependence of the early-type fraction on stellar mass for galaxies in our *luminosity-limited sample* that reside in low-density environments ($\log \Sigma < 0$). Then, for each bin of environment, we determine the morphological fraction predicted by applying this relation to the distribution of stellar masses in that particular environmental bin. The result is a relation between early-type fraction and local density that is due only to the empirical dependence of stellar-mass distribution on environment and morphology on stellar mass, without any direct dependence of morphology on environment. This is shown by the thin, green line in the left panel of Fig. 8.

The variation of the stellar mass function with environment therefore accounts for ~ 40 per cent of the morphology–density relation in our *luminosity-limited sample*. However, this effect has been enhanced by the fact that this sample is limited in terms of absolute-magnitude. At low stellar masses all galaxies in the sample are blue, and preferentially spiral. As we shall see later in this paper, such galaxies exist primarily at low densities. If, rather than an absolute-magnitude limited sample, we use a stellar-mass limited sample, then the contribution to the morphology–density relation due to the varying stellar mass function is reduced. This is

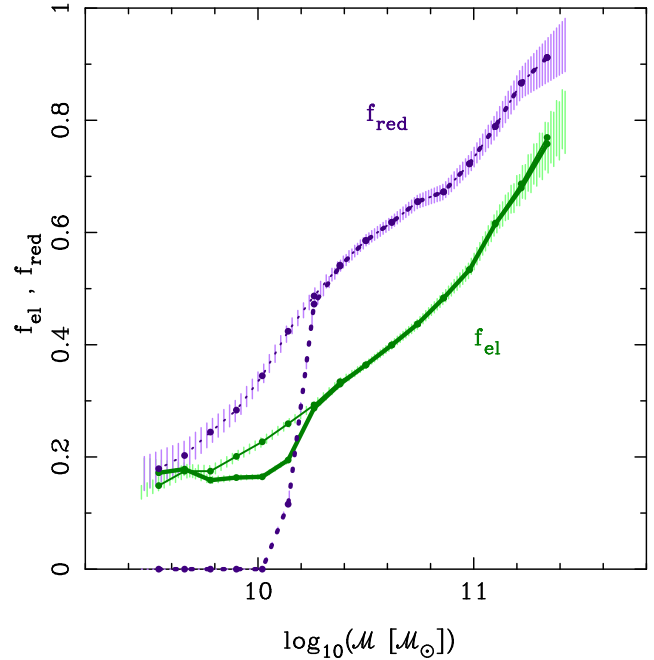


Figure 11. Early-type (green, solid lines) and red (purple, dotted lines) fractions versus stellar mass for galaxies in low-density environments ($\log \Sigma < 0$). In order to fairly sample to low stellar masses we limit the redshift range contributing to each point to ensure completeness. The thick lines show the relation for our *luminosity-limited sample*, while the thin lines give the relation for our *V_{\max} -weighted mass-limited sample*. Note that below $\log(\mathcal{M}_*/\mathcal{M}_\odot) = 10.3$ the absolute magnitude limit of our *luminosity-limited sample* results in an absence of red galaxies, and hence a deficit of early-types. The shaded regions indicate the 2-sigma statistical uncertainties on each equally-spaced $\log \mathcal{M}_*$ bin.

demonstrated using our *V_{\max} -weighted mass-limited sample* (limited to $\log(\mathcal{M}_*/\mathcal{M}_\odot) > 9.8$ and with completeness ensured by a $1/V_{\max}$ correction) in the right panel of 8. Figure 11 shows the relationship of early-type fraction versus stellar mass in low-density environments for both our *luminosity-limited sample* and *V_{\max} -weighted mass-limited sample*. It is these relations, along with the dependence of stellar mass on local density as illustrated in the left panel of Fig. 10, that are used above in determining the contribution of the varying stellar-mass function to the morphology–density relation.

For the *V_{\max} -weighted mass-limited sample*, only approximately 32 per cent of the morphology–density results from the variation of the stellar mass function with environment. The remainder must be due to changes in the early-type fraction with environment at fixed stellar mass. For both samples the morphology–density relation at low densities ($\Sigma \lesssim 1 \text{ Mpc}^{-2}$) is entirely explainable by the environmental variation in the stellar mass function. At greater densities it appears that some process must increase the early-type fraction at fixed stellar mass.

To investigate this in more detail, we utilise our *binned mass-limited sample* to divide our sample into several complete bins of stellar mass (see Sec. 2.2). We make these bins as narrow as reasonable given the uncertainties on the stellar masses. They thus have width 0.2 dex in stellar mass. We only plot alternate bins for clarity. The left panel of Fig. 12 plots the morphology–density relation for several stellar-mass bins. We see that the relations are offset from one another, with the overall fraction of early-types increasing with stellar mass as expected from Fig 11. As we have seen, some of the

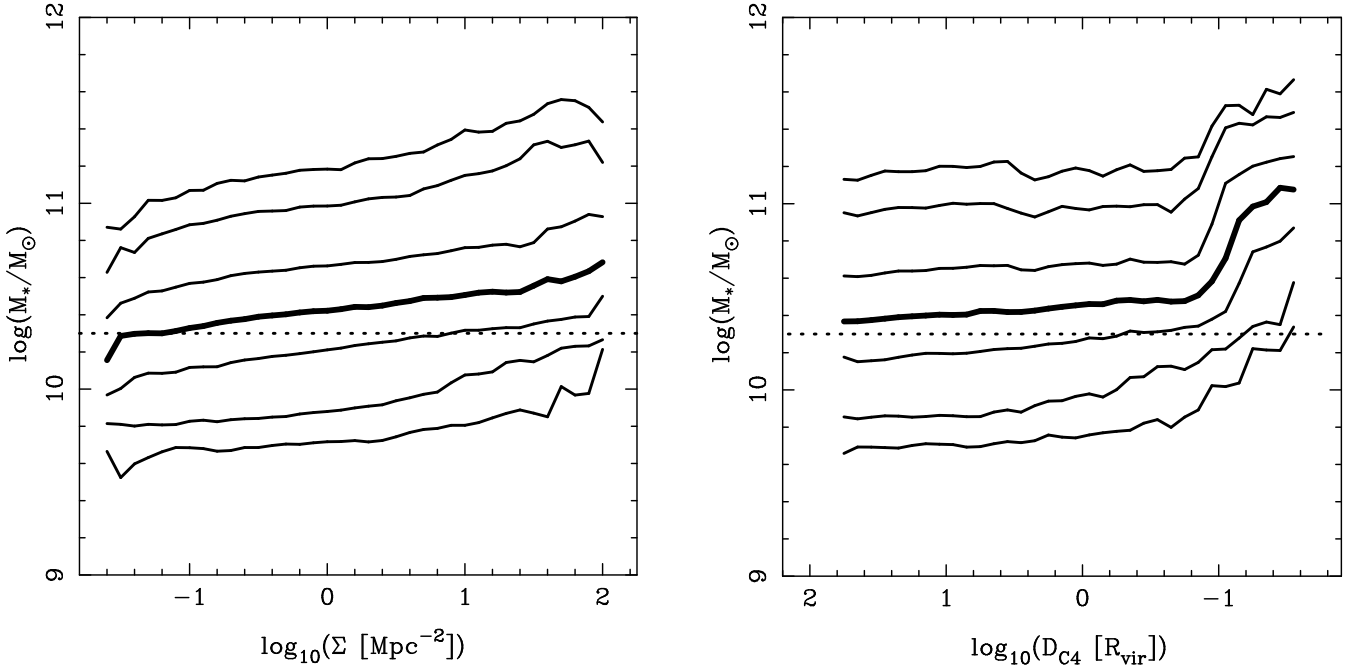


Figure 10. The distribution of stellar mass in our *luminosity-limited sample* as a function of (left) local galaxy density and (right) groupocentric distance. The lines trace the 1, 5, 25, 50 (thick), 75, 95 and 99th-percentiles of the stellar mass distribution in bins of environment. The stellar mass distribution shifts steadily versus local density, while versus groupocentric distance most of the change in the stellar mass distribution occurs within $\sim 0.2R_{\text{vir}}$. The dotted horizontal lines indicate a stellar mass of $10^{10.3}M_{\odot}$, below which our *luminosity-limited sample* becomes incomplete for red galaxies.

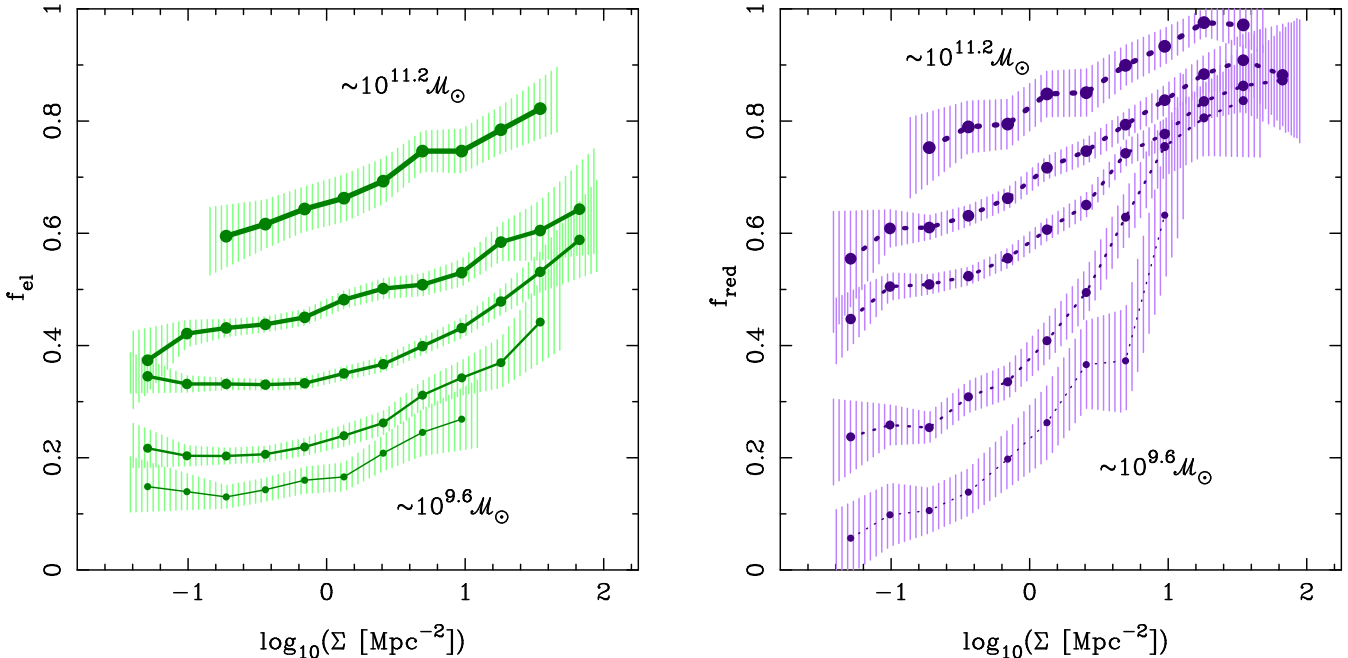


Figure 12. (Left) early-type and (right) red fraction versus local galaxy density for galaxies in selected narrow bins of stellar mass: $\log(M_{*}/M_{\odot}) = 9.5\text{--}9.7$, $9.9\text{--}10.1$, $10.3\text{--}10.5$, $10.7\text{--}10.9$, $11.1\text{--}11.3$, in order from the lowest to highest average f_{el} , f_{red} . The shaded regions indicate the 2σ statistical error on each $\log \Sigma$ bin.

morphology–density relation is due to this effect, in combination with the varying stellar-mass function.

However, a significant trend of morphological fraction with local density is present in each stellar mass bin. The morphology–density relation is not simply a product of a morphology–mass relationship and varying stellar-mass function; it exists even at

fixed stellar mass. This confirms the recent result of van der Wel (2008), which is based on an automatic measure of morphology (Blakeslee et al. 2006), and highlights the difference between morphology and concentration; concentration shows little environmental dependence at fixed stellar mass.

Surprisingly, the change in early-type fraction with environ-

ment is very similar at each stellar mass, being approximately an increase of 0.2 in f_{el} over the local density range probed ($\log \Sigma = -1$ – 1.5). For low stellar masses this corresponds to a doubling of the early-type fraction, while for high masses it is a fractional increase of around a third.

There is a hint that for lower masses the morphology–density relation is flat in low-density environments. For the whole range of masses studied here, $\mathcal{M}_* > 10^{9.5} \mathcal{M}_\odot$, a correlation between early-type fraction and local density is clearly present for $\Sigma \gtrsim 1 \text{ Mpc}^{-2}$, but there is little evidence for a correlation below this density.

3.2 Group properties

In the previous subsection we considered the behaviour of morphological type fraction versus the density of neighbouring galaxies. However, the relative velocities of galaxies in groups and clusters implies that local density may change rapidly, on timescales potentially shorter than those for morphological transformation. The average local density a galaxy experiences is related to the mass of the group halo it resides within. In addition, some proposed mechanisms for environmental galaxy evolution, such as gas starvation and tidal effects, relate directly to global halo properties rather than the local galaxy density. Several studies have thus considered whether galaxy morphology is more fundamentally related to global environmental properties, such as distance to the centre of the nearest galaxy group (groupocentric distance, Whitmore & Gilmore 1991; Whitmore et al. 1993; Gómez et al. 2003; Blanton & Berlind 2007). It would also improve our confidence in our results if the trends can be shown to be independent of the detailed way in which environment is characterised.

To examine the influence of galaxy groups on morphological type fraction we use the C4 group catalogue. The range of local galaxy densities, Σ , covered in groups of varying mass, \mathcal{M}_{C4} , is illustrated by the left panel of Fig. 6. Clearly members of C4 groups reside in regions of high local galaxy density, but the distribution of Σ varies very little across the range of C4 group masses. In Fig. 5 we show the variation of Σ with distance from the centre of the nearest C4 group.

The variation of morphological type fraction versus group mass for C4 group members is plotted in the left panel of Fig. 13. There is no evidence for a change in the early-type fraction over a group mass range of $10^{13} - 10^{15} \mathcal{M}_\odot$. Another estimate of group scale is the integrated red luminosity of the group members (e.g., Lin et al. 2006). As a check we thus additionally show the type fractions as a function of the summed r -band luminosity of all group members with spectroscopic redshifts. There is a slight trend of increasing early-type fraction with increasing group luminosity. However, as versus group mass, this trend is small compared with the trends versus local density. Galaxies at all stellar masses considered in this paper display similarly flat trends versus group mass, simply with offsets due to the dependence of morphology on stellar mass.

In Fig. 14 we show the variation of morphological type fraction versus the distance to the nearest C4 group for our usual *luminosity-limited sample* and *V_{max} -weighted mass-limited sample*. A strong dependence is seen, with the fraction of early-type galaxies increasing for galaxies closer to a group centre. This dependence is particularly strong within the group viral radius, $D_{\text{C4}} \lesssim R_{\text{vir}}$, although a slight trend appears to continue out to larger distances, particularly for the *luminosity-limited sample*. As with density, the relation appears consistent with a smooth function

of groupocentric distance, rather than a broken line as advocated by Goto et al. (2003).

3.2.1 Stellar mass dependence

As was done in Sec. 3.1.1 for local density, we can determine the contribution to the dependence of morphology on groupocentric distance from the environmental variation in the stellar mass function. The stellar mass distribution versus groupocentric distance is illustrated in the right panel of Fig. 10. There is a gradual increase in stellar mass with decreasing groupocentric distance, until $D_{\text{C4}} \sim 0.2 R_{\text{vir}}$, within which the stellar mass distribution rapidly shifts to masses ~ 3 times larger. The exact radius at which this occurs may depend somewhat upon our ‘Fingers of God’ correction (see Appendix B). However, it is clear that galaxies in the cores of groups are typically more massive than those in the field.

We determine the relation between early-type fraction and stellar mass at large groupocentric distances ($\log D_{\text{C4}} > 1$) in each sample, and combine this with the dependence of stellar mass on groupocentric distance. The result is a relation between early-type fraction and groupocentric distance that is due only to the empirical dependence of stellar-mass distribution on environment and morphology on stellar mass, without any direct dependence of morphology on environment. This is plotted as the thin green lines in Fig. 14. Any small trend at large groupocentric distances is attributable to the varying mass function. Below $D_{\text{C4}} \sim 3 R_{\text{vir}}$, however, the early-type fraction increases faster than the mass function can explain. In the cores of groups, $D_{\text{C4}} \leq 0.2 R_{\text{vir}}$, the quickly varying stellar mass distribution causes a similar rise in the early-type fraction, sufficient to account for most of the difference relative to the field. However at intermediate groupocentric distances, the varying mass function is unable to account for any of the increase in early-type fraction. This clearly points to a separate process occurring throughout galaxy groups which increases the early-type fraction at a given stellar mass.

We divide the morphology–groupocentric distance relation into bins of stellar mass in Fig. 15. Due to the smaller number of objects for which we have reliable groupocentric distances, the stellar mass range we can probe with good statistics is less than that for local density. Nevertheless, we can still consider over an order of magnitude in stellar mass. Each stellar mass bin displays a similar trend, with offsets due to the dependence of morphology on stellar mass. At fixed stellar mass there is a small, steady increase in early-type fraction at $D_{\text{C4}} \leq 3 R_{\text{vir}}$, but no evidence for a trend at larger radii.

The trends in morphology with groupocentric distance are very similar to those with respect to local density. As explained in Sec. 2.4, these two ways of characterising environment are measured by different methods and are subject to different interpretational issues. The agreement in the relations of morphology versus both these measures of environment demonstrates that these trends are general and robust.

4 COMPARING MORPHOLOGY AND COLOUR

It is informative to compare the trends of morphology versus environment with those of colour versus environment. As discussed in Sec. 1, morphology is generally considered to be determined by a combination of a galaxy’s dynamical state and star-formation history. Colour is an indicator of a galaxy’s recent ($\lesssim 1 \text{ Gyr}$) star-formation history, with no direct dependence on the spatial dis-

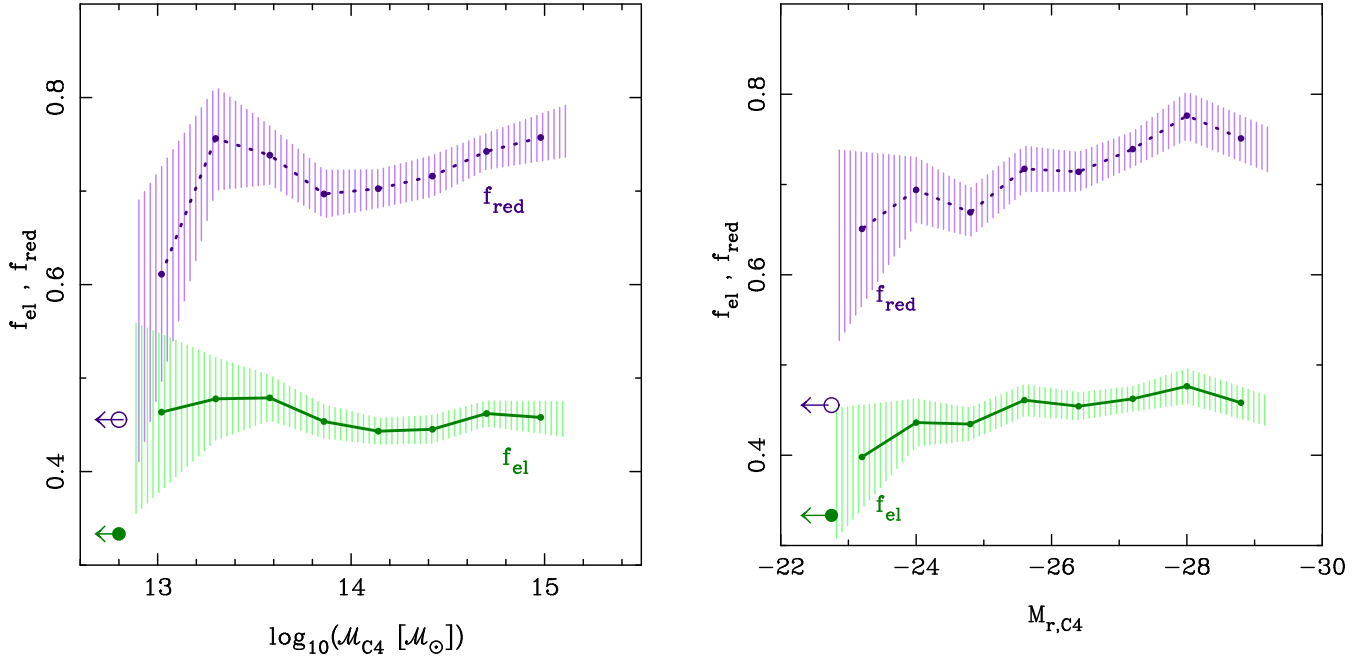


Figure 13. Early-type (green, solid line) and red (purple, dotted line) fractions versus (left panel) group mass and (right panel) integrated r -band group luminosity for members of C4 groups ($D_{C4} < 1R_{\text{vir}}$) in our *luminosity-limited sample*. Only bins containing more than 50 galaxies from at least 5 groups are shown. The shaded region indicates the 2σ statistical error on each equally-spaced bin. The large circles with arrows indicate the mean early-type (filled point) and red (open point) fractions for galaxies that are not members of a C4 group. The early-type fraction is discussed alone in Sec. 3, and compared with the red fraction in Sec. 4.

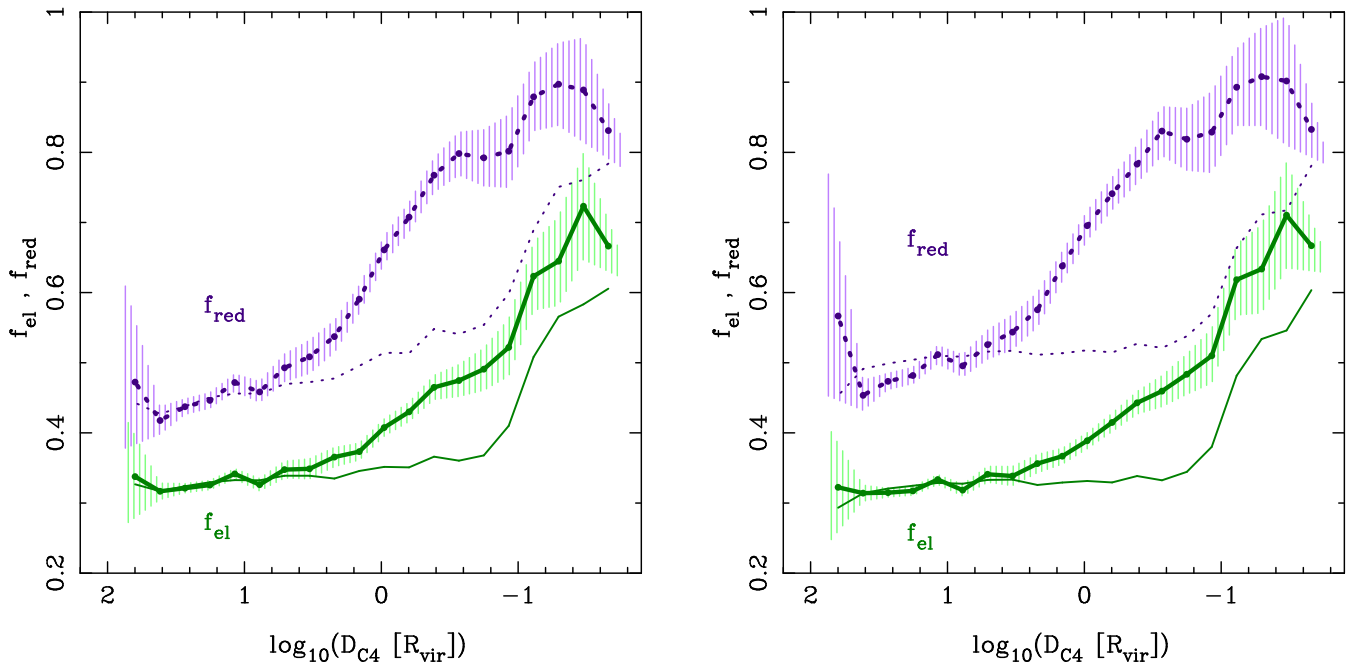


Figure 14. Early-type (green, thick, solid line) and red (purple, thick, dotted line) fractions versus distance to the nearest C4 group normalised by its virial radius, for (left) galaxies in our *luminosity-limited sample* and (right) our V_{max} -weighted *mass-limited sample*, complete for stellar masses $\log(\mathcal{M}_*/\mathcal{M}_\odot) > 9.8$, and constructed by applying $1/V_{\text{max}}$ weightings to our *magnitude-limited sample* (see Sec. 2.2). The shaded regions indicate the 2σ statistical error on each equally-spaced $\log D_{C4}$ bin. Note that in this and subsequent plots the $\log D_{C4}$ axis is plotted with positive values on the left and negative values on the right for easier comparison with the plots versus Σ . The right-most $\log D_{C4}$ bin additionally includes all galaxies with lower $\log D_{C4}$. Thin lines show the contribution to each relation attributable to variation in the stellar mass function with environment (see Sec. 3.2.1). The early-type fraction is discussed alone in Sec. 3, and compared with the red fraction in Sec. 4.

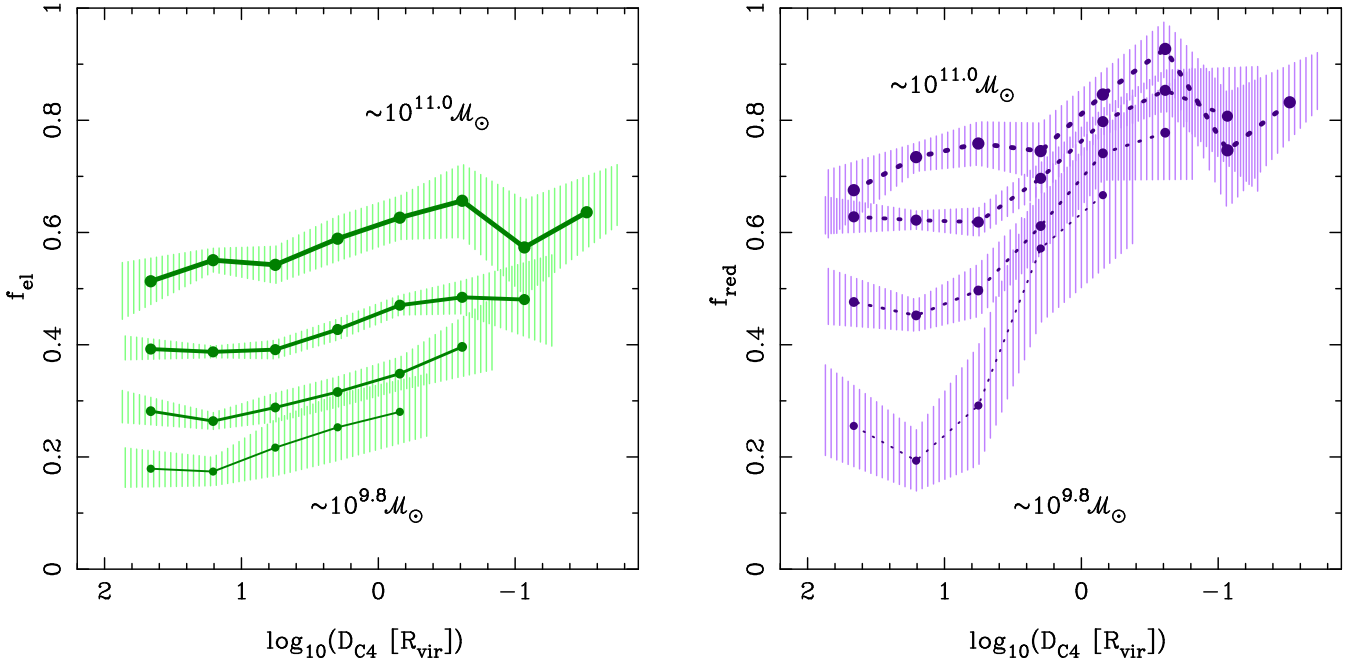


Figure 15. (Left) early-type and (right) red fraction versus distance to the nearest C4 group normalised by its virial radius, for galaxies in narrow bins of stellar mass: $\log(\mathcal{M}_*/\mathcal{M}_\odot) = 9.7\text{--}9.9$, $10.1\text{--}10.3$, $10.5\text{--}10.7$, $10.9\text{--}11.1$, in order from the lowest to highest average f_{el} . The shaded regions indicate the 2σ statistical error for each $\log D_{\text{C4}}$ bin. For each stellar mass range, the right-most $\log D_{\text{C4}}$ bin additionally includes all galaxies with lower $\log D_{\text{C4}}$.

tribution of its stars. Differences in the behaviour of colour and morphology with environment will thus give indications of the environmental mechanisms at work.

Several previous studies have addressed this issue using automatic morphology proxies. Those which consider structural measures of morphology, such as concentration or Sersic index, find that these quantities are much less dependent upon environment than they are on galaxy mass (Kauffmann et al. 2004; Hogg et al. 2004). In contrast, colour and star-forming fractions are strongly dependent upon both environment and mass (Baldry et al. 2006). However, van der Wel (2008) has shown that using a more sophisticated morphology proxy, which accounts for the presence of ‘bumpiness’ in the surface-brightness distribution, leads one to conclude that morphology is more dependent on environment than mass. Different morphological and structural measurements thus lead to apparently opposing conclusions. With the Galaxy Zoo dataset we can address these issues using traditional visual morphologies, without recourse to automatic proxies. As discussed in Sec. 1, visual morphology is primarily concerned with azimuthal structure, i.e. spiral arms, which are not well characterised by proxies, and which contains different information to that provided by radial structural measurements.

In order to compare how colour and morphology depend on environment we must adopt a measure of colour and a criterion for dividing objects into red and blue samples. We follow Baldry et al. (2006), using the optimal, stellar-mass-dependent, divider they determine to separate galaxies based on the bimodality of the $u - r$ colour distribution. This utilises the SDSS model magnitudes (Stoughton et al. 2002), and therefore the colour is effectively centrally weighted. We simply class objects above and below the Baldry et al. divider as ‘red’ and ‘blue’, respectively. We do not attempt to work with likelihoods of whether individual galaxies lie on the red or blue sequence, though this is possible by assuming the Gaussian fits of Baldry et al..

Figure 8 plots both the early-type and red galaxy fractions versus local galaxy density, for our *luminosity-limited sample* (complete for $M_r < -20.17$), on the left, and *V_{max} -weighted mass-limited sample* (complete for $\log(\mathcal{M}_*/\mathcal{M}_\odot) > 9.8$), on the right. We see that the qualitative trends for morphology and colour are similar, but the morphology–density and colour–density relations are offset from one another. Averaging over our *luminosity-limited sample* the fraction of red galaxies which have early-type morphology is 67 per cent. However, the differences in the shape of the early-type and red fraction trends in Fig. 8 demonstrate that this fraction is a function of environment. It is clear that morphology and colour are not equivalent ways of classifying galaxies, and that they are not equally affected by environment. We shall explore this further below.

Moving onto group properties, the left panel of Fig. 13 shows that, as was seen for early-type fraction alone in the previous section, there is no clear trend of red-fraction with group mass. The right panel indicates a small trend versus the summed r -band luminosity of group members, though this is small compared with the variation with environment and, as we shall see below, stellar mass. Blanton & Berlind (2007) find a strong variation of red fraction with group luminosity. However, this is driven by lower group masses than we consider here. At high group masses their red fractions match ours. This also agrees with Poggianti et al. (2006) who find that for SDSS groups with $\gtrsim 10^{13.4} \mathcal{M}_\odot$ (assuming the velocity dispersion to mass conversion given by eqn. 2 of Biviano et al. 2006) there is no mass-dependence of the star-forming fraction, while below this there is a clear dependence. Interestingly, they also show that the plateau of star-forming fraction in high-mass groups has only set in since $z \sim 0.6$.

Earlier we showed that the early-type fraction is closely related to the groupcentric distance. In Fig. 14 we show that this is also true for the red fraction. The fraction of red galaxies with early-type morphology varies strongly with groupcentric distance.

As for density, however, there is a considerable difference in the red and early-type relations versus groupcentric distance, in terms of both an offset and the shape of the dependence.

As was done earlier for morphology (see Sec. 3.1.1), we determine the contribution to the relations between colour and environment due to trends in the distribution of galaxy stellar masses versus environment. The relations between red fraction and stellar mass for low density environments in our data is shown in Fig. 11, for both our *luminosity-limited* and *V_{\max} -weighted mass-limited* samples. The trends of colour versus environment expected from these relations, combined with the environmental dependence of stellar mass (Fig. 10), are indicated by the thin, dotted lines in Fig. 8 & 14, for density and groupcentric distance, respectively. We find that, as for morphology, the varying stellar mass function is inadequate to explain the rapid increase in the red fraction at intermediate to high local densities, and at intermediate groupcentric distances. Again, this is plain evidence for an environmental process at work in groups.

In low density environments we have seen that any morphology–environment relation can be explained by the dependence of the stellar mass function on environment. In contrast, for colour there is a strong indication of a residual trend versus both density and groupcentric distance. The slope of the colour–environment relations expected due to the varying stellar mass function is not as steep as that observed. This strongly suggests that, while morphology is unaltered, colour is significantly affected by environmental variation at low densities. Studies of galaxies in void environments have previously found colour, and star formation, to vary with local galaxy density (Rojas et al. 2004, 2005; Ceccarelli et al. 2008). Figures 8 & 14 clearly demonstrate that this effect is in addition to that expected from the varying stellar mass function, and that it is not related to changes in the ratio of early-types to spirals.

4.1 Stellar mass dependence

The colour–density and colour–groupcentric distance relations for narrow bins of stellar mass are shown in the right panels of Fig. 12 & 15, respectively. As Baldry et al. (2006) have shown, the red fraction depends strongly on environment at fixed stellar mass, particularly for low masses ($< 10^{10} M_{\odot}$), for which the red fraction varies from < 0.2 to > 0.8 between low and high-density environments. This is in excellent agreement with Haines et al. (2006) who find that the relation between star-formation history and environment is very different for giant and dwarf galaxies (roughly above and below $\sim 10^{9.5} M_{\odot}$, respectively). However, rather than a sharp division between giant and dwarf galaxies, we see a continuous, though rapid, decrease in the sensitivity of red fraction to environment with increasing stellar mass.

The dependence of red fraction on environment and stellar mass contrasts with the trends for early-type fraction shown in the left panels of these figures. The early-type and red fractions vary similarly with environment at high masses, but for low masses colour is much more sensitive to environment. The shapes of the environmental dependences also differ, with the morphology relations displaying their largest gradients at the highest densities and smallest groupcentric distances, whereas the colour relations rise most rapidly at intermediate densities and groupcentric distances, and flatten off in the densest environments.

As mentioned earlier for morphology alone, the agreement of the relations versus groupcentric distance and local galaxy density demonstrate the robustness of these trends in galaxy properties with

respect to a general definition of environment. We will consider the detailed differences between the morphological and colour trends with respect to these two environmental measures in a subsequent paper.

In this paper, we focus our investigation on the transformation of galaxies due to environmental mechanisms. However, it is apparent that many massive galaxies are red and have early-type morphology independent of their environment. For some reason their star formation has ceased, and in many cases their stellar dynamics have become dominated by random motions, without an obvious environmental cause. Some of these galaxies may be fossil groups (Jones et al. 2003), and hence only appear to be in low-density environments. However, in any case, such massive, isolated galaxies are likely to be centred in a gaseous halo, which should be supplying them with fuel for star formation. Preventing gas-cooling, and hence star formation, in massive galaxies remains a puzzle, although active galactic nuclei (AGN) may play a significant role (Croton et al. 2006; Bower et al. 2006; Croton & Farrar 2008). There is even a possibility that AGN activity could directly affect the morphology of galaxies (Fan et al. 2008). However, AGN are only powerful enough to have a significant impact in massive galaxies. Furthermore, AGN activity is unlikely to depend directly upon environment, although in principle AGN activity may vary as a result of the same environmental processes that affect star formation. Haines et al. (2007) investigate the relative importance of AGN versus environmental mechanisms for preventing star formation in galaxies of different masses.

It is often implicitly assumed that the red population corresponds to objects with early-type morphology, and that blue corresponds to spiral. While this is correct for the majority of objects, making the assumption that these correspondences hold true in general can be highly misleading. The differences between the red and early-type fractions imply the existence of substantial populations of ‘unconventional’ galaxies: red spirals and blue early-types. Furthermore, the contrast between their dependences versus both environment and stellar mass require that these ‘unconventional’ populations are not a constant contaminant, but vary strongly. One cannot, therefore, make inferences about the environment and mass dependences of morphology from a consideration of colour alone.

We now examine the dependence of the red spiral and blue early-type populations on environment and stellar mass.

4.2 Red spirals and blue early-types

In the left panels of Fig. 16 & 17 we plot the fraction of galaxies that meet our red spiral and blue early-type criteria as functions of local galaxy density and groupcentric distance, respectively. We continue to derive morphological type fractions directly from the debiased Galaxy Zoo type likelihoods. Here we simply modify these for ‘red spirals’ by reducing the likelihood to zero for those objects bluer than the Baldry et al. (2006) divider. Likewise, for ‘blue early-types’ we remove objects redder than the colour divider.

The fraction of red spirals displays a clear peak versus both local density and groupcentric distance. In low density regions and far from C4 groups, red spirals constitute ~ 16 per cent of the local galaxy population brighter than $M_r < -20.17$. This fraction almost doubles with increasing local density or decreasing groupcentric distance, rising to a peak of ~ 28 per cent at ~ 6 galaxies Mpc^{-2} or $\sim 0.4R_{\text{vir}}$. At higher densities or in the cores of groups the red spiral fraction declines sharply.

The fraction of blue early-types simply diminishes steadily from ~ 12 per cent to ~ 2 per cent from the least dense to most

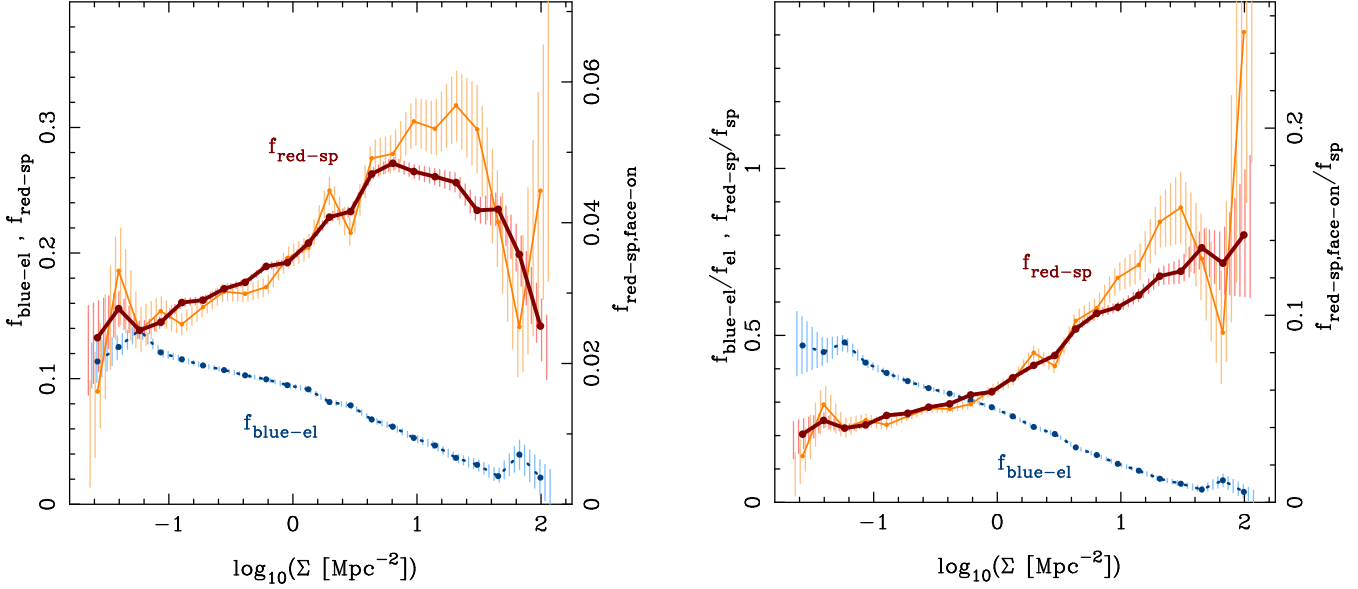


Figure 16. The number of red spirals (red, thick, solid line) and blue early-types (blue, dotted line) in our *luminosity-limited sample* versus local galaxy density (left) as fractions of our whole sample and (right) as fractions of all spirals and early-types, respectively. Also shown for comparison is the fraction of face-on red spirals (orange, thin, solid line), scaled to have the same mean fraction as the full red spirals sample, as indicated by the scale on the right of the plot. The shaded regions indicate the 2-sigma statistical uncertainties on each $\log \Sigma$ bin.

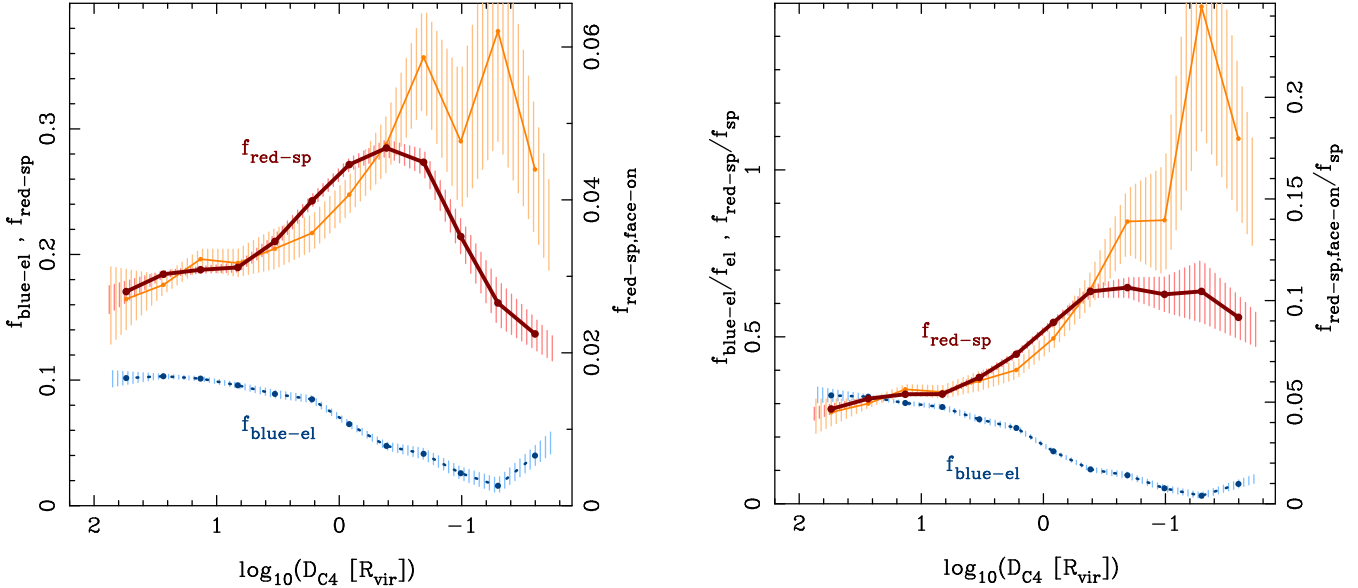


Figure 17. The number of red spirals (red, thick, solid line) and blue early-types (blue, dotted line) in our *luminosity-limited sample* versus distance to the nearest C4 group normalised by its virial radius (left) as fractions of our whole sample and (right) as fractions of all spirals and early-types, respectively. Also shown for comparison is the fraction of face-on red spirals (orange, thin, solid line), scaled to have the same mean fraction as the full red spirals sample, as indicated by the scale on the right of the plot. The shaded regions indicate the 2-sigma statistical uncertainties on each $\log D_{C4}$ bin. The right-most $\log D_{C4}$ bin additionally includes all galaxies with lower $\log D_{C4}$.

dense environments. The extreme members of this population are studied in detail by Schawinski et al. (2008), and are also found to preferentially inhabit low-density environments. Schawinski et al. (2007) have also previously shown that the fraction of blue early-types declines with local galaxy density. The blue colours of these galaxies indicates that they have recently formed significant numbers of new stars, in contrast to the usual picture of early-types as ‘red and dead’. By using UV–optical colours, Schawinski et al. (2007) have shown that over 30 per cent of bright ($M_r < -21.5$)

early-types have recently formed stars. Our fractions are lower, due to the lower sensitivity of the $(u - r)$ colour used in this paper to low levels of recent star formation, but still substantial, and trace the same environmental dependence.

For both red spirals and blue early-types there is little evidence for any dependence on groupcentric distance beyond $\sim 5R_{\text{vir}}$. As previously, we find very little dependence of group members on the mass of the group in which they reside, over the range $10^{13.4} -$

$10^{15.2} M_{\odot}$. The fraction C4 group members which are red spirals or blue early-types is flat at ~ 26 and ~ 6 per cent, respectively.

What we have discussed so far, and plotted in the left panels of Fig. 16 & 17, is the fraction of all galaxies that are either red and spiral or blue and early-type. This quantity indicates the environments in which these objects contribute most significantly to the overall galaxy population. However, it is also informative to consider the fractions of spirals that are red, and early-types that are blue, as the spiral and early-type fractions are themselves strong functions of environment. These ‘type normalised’ fractions are plotted in the right panels of Figs. 16 & 17 as functions of local density and groupocentric distance, respectively.

The environmental dependence of the fraction of spirals that are red is simpler than the fraction of the whole galaxy population that are red and spiral. We now see that the decline in the fraction of red spirals at high densities, and in the the cores of groups, is a result of the declining spiral fraction. The fraction of spirals that are red increases steadily to the highest local densities. The dependence versus groupocentric distance is most interesting, as it appears localised to a range of radii. Between 0.4 and $6R_{\text{vir}}$ the fraction of spirals that are red doubles, while outside of this range it is constant. A similar behaviour is seen for the fraction of early-types that are blue, with a two-thirds decline over the same groupocentric distance range.

To gain further insight into the behaviour of the red spiral and blue early-type populations with environment, we again utilise our *binned mass-limited sample* and split our sample into complete, narrow bins of stellar mass. Figures 18 & 19 plot the fractions of spirals that are red and early-types that are blue for these stellar mass bins, versus local galaxy density and groupocentric distance, respectively.

At all stellar masses there is a trend in the fractions of spirals that are red and early-types that are blue versus environment. In low density environments these fractions are strong functions of stellar mass. In these environments, at high stellar masses, $\mathcal{M}_{*} \gtrsim 10^{11} M_{\odot}$, the majority of spirals, and almost all early-types, are red; at low stellar masses, $\mathcal{M}_{*} \lesssim 10^{9.6} M_{\odot}$, almost all galaxies are blue, irrespective of their morphology. This corresponds with the finding of Conselice (2006) that the correlation between galaxy colour and stellar mass does not strongly depend on morphology. It does, however, depend strongly on environment. The environmental dependence for low mass galaxies is much stronger than for high mass galaxies, such that in high density environments ($\Sigma > 10 \text{ Mpc}^{-2}$, $D_{\text{C4}} < 0.3R_{\text{vir}}$) 80 per cent of spirals and 90 per cent of early-types are red, irrespective of their stellar mass. In dense environments the fractions of spirals that are red and early-types that are blue are therefore only weak functions of stellar mass.

4.2.1 S0 galaxies and red spirals

We see a significant fraction of red spirals in the field, particularly at high stellar masses. This results from a lack of correspondence between the morphology and colour bimodalities (van den Bergh 2007), which is present across all environments. Many massive galaxies appear on the red side of the colour bimodality, irrespective of their morphology. As shown in appendix A of James et al. (2008), with typical selections one finds that half to two-thirds of Sa galaxies are red. Maller et al. (2008) have also shown that many red (and concentrated) objects are truly disk galaxies. These would often be mistakenly considered to be early-types in studies using colour and concentration as proxies for morphology. About one-

third of these objects are red simply due to being orientated edge-on and thus suffering from significant dust reddening.

A substantial fraction of the red spiral population we have identified shows a strong dependence on environment, preferentially occurring in intermediate local densities and within the virial radius, but not the cores, of galaxy groups. It is unclear whether our red spiral sample comprises only similar objects, which display only limited environmental variation, or whether it is made up from several distinct populations with different environmental dependences. However, we do not see any change in the fraction of red-spirals that are classified as edge-on/unclear as a function of environment. Thus, the environmental trends cannot simply be attributed to a change in the proportion of red-spirals that are selected without having clearly visible spiral arms.

S0 galaxies possess discs and are generally found to have little star formation and to be red in colour. They are also known to preferentially inhabit clusters, especially at low redshifts (e.g., Dressler 1980b). This morphological type is not explicitly identified in the current Galaxy Zoo classification scheme, and S0s are thus distributed between the early-type and spiral classes in an uncertain manner. There is therefore a concern that the environmental behaviour we have found for red spirals may simply be due to the S0 population. However, recall that Fig. 4 demonstrates that almost all the objects classified as E/S0 or S0 by F07 have low spiral likelihoods in Galaxy Zoo. These objects therefore contribute very little to the spiral fraction. Objects classified by F07 as S0/Sa also generally have low spiral likelihoods, and many of these, especially those with higher spiral likelihoods, may be better classified as spiral rather than S0, as they must have a suggestion of spiral arms. It is thus apparent that the red spirals we discuss above are an additional population to the S0s considered in many other studies.

There remains the possibility that Galaxy Zoo, F07, and thus presumably most other studies, mistakenly classify a significant fraction of edge-on S0s as spirals. In Galaxy Zoo we can ask the question of whether objects were classified as spiral due to the presence of visible spiral arms or simply due to a disky, edge-on appearance. We define as ‘edge-on/unclear’ those objects for which the majority of Galaxy Zoo classifiers could not individually discern a spiral arm direction ($p_{\text{CW}} + p_{\text{ACW}} < p_{\text{EU}}$ where CW, ACW and EU refer to clockwise, anti-clockwise and edge-on/unclear, respectively). Note that this is conservative, as if even a minority of classifiers can discern spiral arms in a galaxy then it is very likely to be a spiral. The classification bias correction (see Appendix A) increases the spiral likelihood for such objects when they have apparent luminosities or sizes which may make distinguishing them from early-types difficult. The spin likelihoods ($p_{\text{CW}}, p_{\text{ACW}}, p_{\text{EU}}$) have not been corrected for such biases, and simply reflect the proportion of user classifications. Spiral galaxies may therefore include a surprisingly high fraction of edge-on/unclear objects, given the above definition.

For all objects that are more likely to be spirals than anything else ($p_{\text{sp,adj}} > 0.5$), the fraction of edge-on/unclear objects is 55 per cent, while for red spirals it is 81 per cent. There are three possible reasons for this discrepancy: (a) edge-on spirals suffer from greater dust-reddening, so will be more prevalent in a red sample; (b) due to the connection between star formation and spiral arms, objects with low specific star-formation rates will tend to be red and have lower spiral arm contrast, and are thus more likely to be classified as edge-on/unclear; and (c) a fraction of objects classified as edge-on/unclear spirals are actually S0 galaxies, with typically redder colours. For cases (b) and (c), there must be a population of these objects viewed closer to face-on and hence classified as

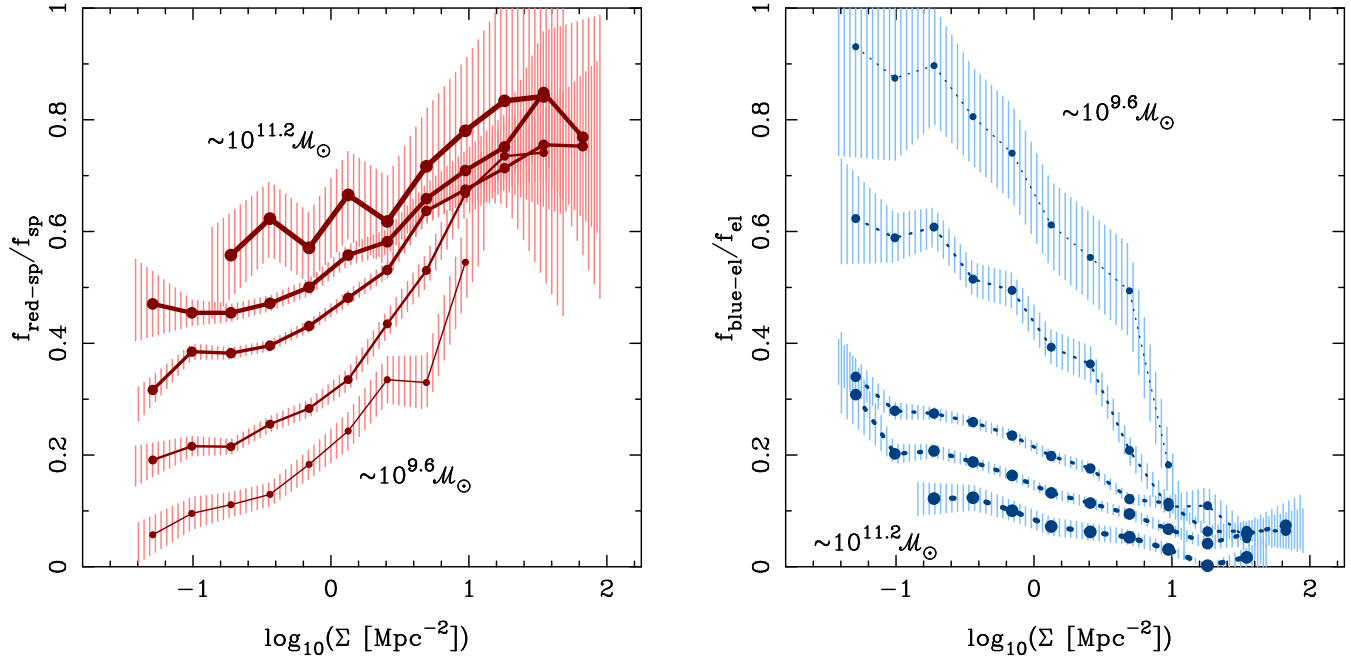


Figure 18. The fraction of (left) spirals that are classified as red galaxies, and (right) early-types classified as blue galaxies, plotted as a function of local galaxy density, for our *binned mass-limited sample*: $\log(\mathcal{M}_*/\mathcal{M}_\odot) = 9.5\text{--}9.7, 9.9\text{--}10.1, 10.3\text{--}10.5, 10.7\text{--}10.9, 11.1\text{--}11.3$. The shaded regions indicate the 2-sigma statistical uncertainties on each $\log \Sigma$ bin.

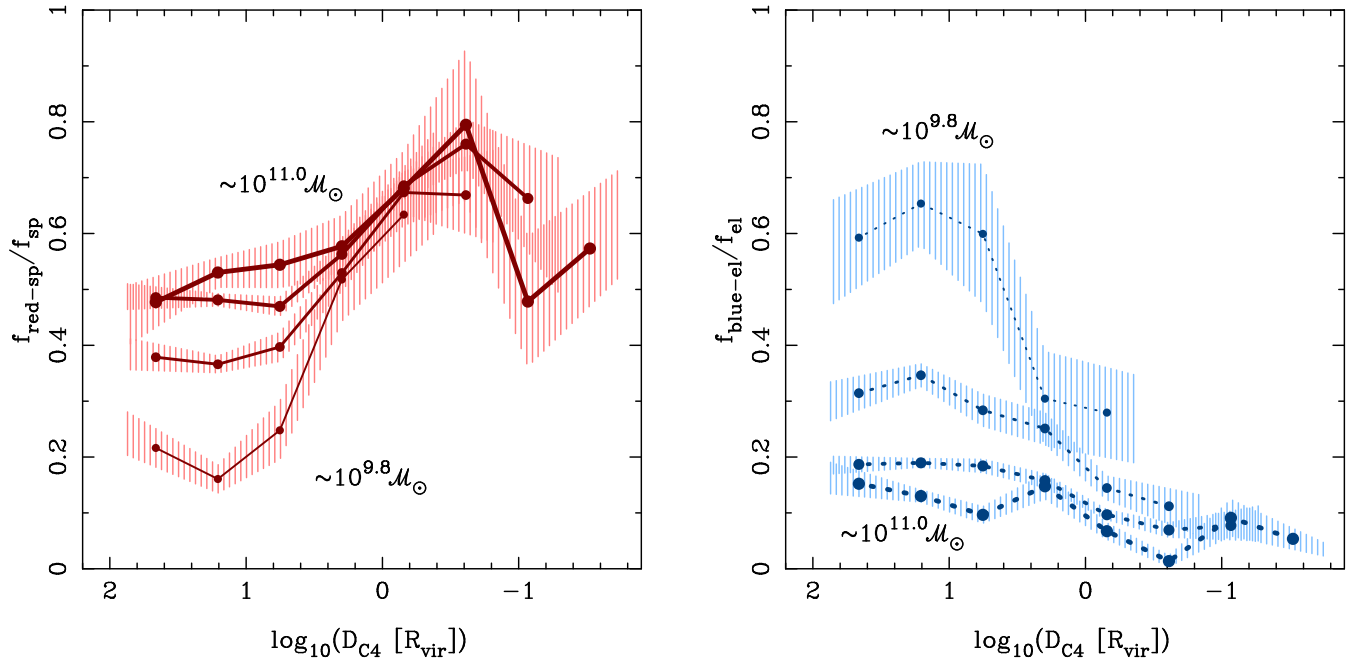


Figure 19. The fraction of (left) spirals that are classified as red galaxies, and (right) early-types classified as blue galaxies, plotted as a function of groupcentric distance, in our *binned mass-limited sample*: $\log(\mathcal{M}_*/\mathcal{M}_\odot) = 9.7\text{--}9.9, 10.1\text{--}10.3, 10.5\text{--}10.7, 10.9\text{--}11.1$. The shaded regions indicate the 2-sigma statistical uncertainties on each $\log D_{C4}$ bin.

early-type. The environmental trends we see in a fraction of the red spirals must correspond to some combination of environmental variations in the (a) dust-content, (b) star-formation rate, and (c) S0 contamination of the spiral galaxy population.

Edge-on/unclear spirals are, in the median, 0.29 mag redder than galaxies with clearly visible spiral arms (in $(u-r)_{\text{model}}$, relative to the stellar-mass-dependent divider of Baldry et al. 2006).

However, determining whether this is due to extinction affecting otherwise normal spiral galaxies, or due to older luminosity-weighted stellar populations, is beyond the scope of this paper.

For 19 per cent of our red spirals significant spiral arms are seen by a majority of classifiers, and the true fraction with spiral arms, including those undetected in Galaxy Zoo, must be higher. At least a fifth of our red-spiral population must therefore be true spi-

rals, not S0 galaxies. We can check that these face-on spirals, which we are certain possess spiral arms, behave in the same manner as our whole red spiral population. This is shown by the orange lines in Figs. 16 & 17, which plot the fractions for face-on red spirals only, scaled by the ratio of all red spirals to face-on red spirals. As a function of local density, the fraction of face-on red spirals behaves very similarly to the full red spiral sample. Versus groupcentric distance they also behave similarly, except within $D_{C4} \lesssim 0.4R_{\text{vir}}$, where there is an excess of face-on red spirals compared with the full red spiral population. This suggests that in groups edge-on red spirals are less likely to be classified as spirals than they are in the field. This is interesting in itself, but here we simply stress that this implies that our red spiral population is not dominated by S0s in groups, rather there may be proportionally fewer S0s in our red spiral sample in dense regions. A substantial fraction of our red spiral population thus appears to comprise galaxies with significant spiral arm structure, even if many are seen edge-on.

As explained in Sec. 2.1, the colours used in this study are based on SDSS model magnitudes. They are thus sensitive to the dominance of the bulge component of a disc galaxy. In contrast, the Galaxy Zoo morphologies are sensitive to the presence of spiral arms or an edge-on disk, even when the galaxy light is dominated by a bulge. This is because the images were displayed for classification using a non-linear (arcsinh) stretch, as described in Lupton et al. (2004). Other photometric apertures, such as Petrosian, may give colours that are more representative of the overall galaxy, and so which may be more suitable for identifying galaxies with red discs. Measuring colour in an annular aperture may be most appropriate for this purpose (Park et al. 2007). The choice of other photometric bands (e.g., $g - r$) and dividing lines in the colour–magnitude diagram may somewhat modify the trends shown. However, we do not expect the overall behaviour of the red-spiral population versus environment to depend dramatically upon our choice of colour.

4.2.2 Breaking down the dependence of red fraction on environment

Having studied the relationship between morphology and environment, and the environmental variations in the fractions of early-types and spirals that are red, we are now in a position where we can identify the various contributions to the dependence of red fraction on environment.

The red fraction can be written as a sum of contributions from red spirals and red early-types:

$$f_{\text{red}} = \frac{f_{\text{red-sp}}}{f_{\text{sp}}} f_{\text{sp}} + \left(1 - \frac{f_{\text{blue-el}}}{f_{\text{el}}}\right) f_{\text{el}}. \quad (1)$$

We have already determined f_{sp} , f_{el} , $f_{\text{red-sp}}/f_{\text{sp}}$ and $f_{\text{blue-el}}/f_{\text{el}}$, as functions of density. To assess the red fraction resulting from the morphology–density relation we simply set $f_{\text{red-sp}}/f_{\text{sp}}$ and $f_{\text{blue-el}}/f_{\text{el}}$ to their average values in Eqn. 1, while allowing f_{sp} and f_{el} to vary with density. The contribution from the changing fraction of spirals that are red is found by holding all terms except $f_{\text{red-sp}}/f_{\text{sp}}$ constant at their mean values. Finally, by holding all terms except $f_{\text{blue-el}}/f_{\text{el}}$ at their mean values we determine the contribution from the environmental variation in the fraction of early-types which are blue.

These contributions to the relation between red fraction and local density, for our *luminosity-limited sample*, are plotted in the left panel of Fig. 20. In order to examine only trends, rather than

absolute values, we normalise each curve to the mean value of the three lowest density bins. The most striking result of this exercise, though already partly clear from Fig. 8, is that the morphology–density relation is responsible for very little of the colour–density relation. The modest increase in the early-type fraction with local density is not enough to explain the much larger increase in red fraction. Furthermore, as the early-type and spiral populations both contain significant fractions of red galaxies, which increase to comparable proportions in dense environments, the rise in the early-type fraction with density has surprisingly little effect on the red fraction. The colour–density relation is driven by changes in the red fraction at fixed morphology, i.e. the fraction of early-types and spirals that have red colours. In low density environments the rise of red spirals and fall of blue early-types contribute similarly. At higher densities the rapidly increasing red spiral fraction is the dominant contribution to the colour–density relation.

Note that the variation of the stellar mass function with environment is still present in Fig. 20. Its influence will be shared amongst the various contributions, for as we have seen, early-type fraction and the fraction of early-types and spirals that are red depend strongly on stellar mass (Fig. 12 and Fig. 18).

The relative importance of the red spiral population varies with stellar mass. To show this we determine the contribution to the colour–density relation over the range $\log \Sigma = 0.8\text{--}1.5$ in narrow bins of stellar mass. These are shown in the right panel of Fig. 20. Using narrow stellar mass bins also has the advantage of removing the effect of environmental variations in the stellar mass function. Red spirals dominate the colour–density relation at low stellar masses, but at high masses red spirals, blue early-types, and the morphology–density relation contribute equally.

4.2.3 Why are galaxies red in dense environments?

Our red spirals, and particularly the portion which are prevalent in the outskirts of galaxy groups, bear a strong resemblance to populations discussed by a number of previous studies. These include the anaemic spirals of van den Bergh (1976), the passive spirals identified by Goto et al. (2003) and confirmed by Yamauchi & Goto (2004), H α truncated (e.g., Koopmann & Kenney 2004) and HI-deficient spirals (e.g., Vogt et al. 2004). More recently Lane et al. (2007) have studied a population of dusty, red spirals associated with the intermediate density regions in a supercluster, which Wolf et al. (2007) and Wolf et al. (2008) find to still be hosting low levels of highly-obscured star formation. All of these populations are obviously closely related, and their memberships must overlap considerably. However, the various selections may highlight objects at different stages of an evolutionary sequence, or subject to the action of different mechanisms. In general, most of these red spiral populations appear to result from the removal of gas from the haloes and/or discs of normal spiral galaxies in cluster and group environments.

Considering Fig. 16, one might conclude that a more general, rather than a group-specific, mechanism is responsible for the environmental variation in the red spiral fraction. This is implied by the finding that the slope of the red-spiral fraction versus local density relation declines smoothly and does not entirely flatten-off at low densities. For example, such a conclusion is reached by Balogh et al. (2004) due to a similar behaviour of the star-forming fraction versus local density. However, when considering groupcentric distance as the environmental indicator, in Fig. 17, we see that almost all the variation in the red-spiral fraction occurs within a few R_{vir} . The mass of the group involved does not signif-

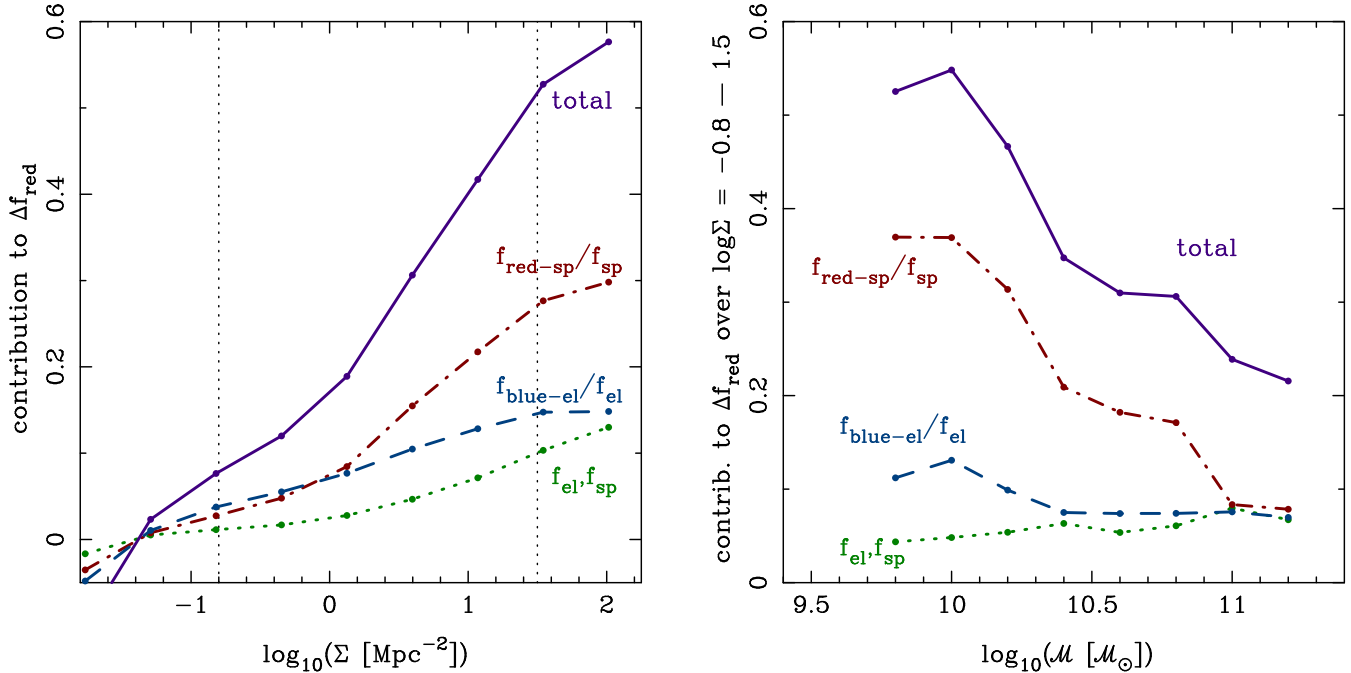


Figure 20. (Left) the change in the red fraction of galaxies in our *luminosity-limited sample*, divided into contributions due to the variation with local density of the morphological type fractions (green, dotted line), the fraction of spirals that are red (red, dot-dashed line) and the fraction of early-types that are blue (blue, dashed line). The total colour–density trend is shown by the solid, purple line. (Right) the contributions to the change in red fraction over the local density range $\log \Sigma = 0.8\text{--}1.5$ as a function of stellar mass (indicated by the vertical dotted lines in the left panel).

icantly affect the red-spiral fraction, at least above some threshold which lies below the range of group masses considered in this paper ($\gtrsim 10^{13} M_{\odot}$).

Recall from Fig. 6 that there is a spread of local density for group members: and thus a sharp transition in groupcentric distance will result in a smoother variation with respect to local density. This argument suggests that the majority of the environmental dependence of red-spirals is due to group membership, rather than local density, and hence that a significant proportion of red spirals are a result of group-specific mechanisms.

In the cores of groups, many galaxies have early-type morphology and red colours. Much of this can be explained by a shift of the stellar mass function to higher masses in these regions, together with the higher early-type and red fractions for more massive galaxies (Figs 10 & 11). However, this does not help to explain the high early-type and red fractions in the outskirts of groups. At a given stellar mass the early-type fraction is higher in dense environments. This indicates that some process must have created early-types preferentially in dense regions, either at the epoch of galaxy formation or subsequently. A recent direct study of evolution in the morphology–density relation by van der Wel et al. (2007) demonstrates that the relation has not significantly changed out to $z \sim 1$, when one considers a mass-selected sample. The evolution found by previous studies (Smith et al. 2005; Postman et al. 2005) is attributed to effects of their luminosity-based selection. The star-formation properties of galaxies in dense regions appears to have changed, while their morphologies have not. This is at odds with the picture of spirals transforming to S0s in clusters (Dressler et al. 1997; Bedregal et al. 2006; Aragón-Salamanca et al. 2006; Barr et al. 2007; Desai et al. 2007). However, this picture remains contentious, with other studies concluding that luminous S0s cannot have formed from faded spirals because of their larger bulge sizes and luminosities, rel-

ative to those of spirals (Burstein 1979; Dressler 1980b; Gisler 1980; Christlein & Zabludoff 2004; Boselli & Gavazzi 2006). The study of van der Wel et al. (2007) is limited to massive galaxies ($M_{*} \lesssim 10^{10.6} M_{\odot}$), so there is still room for the morphology–density relation to evolve at lower masses.

The significant population of red spirals we identify, which preferentially reside in the outskirts of groups, are predominantly of intermediate stellar mass. Furthermore, the lowest mass objects appear to be those which are most strongly affected by their environment, as in the field they are almost all blue. The star formation in these objects must have declined recently, within the past few Gyr, in order for their spiral arms to remain with sufficient contrast to be visible. Indeed, Wolf et al. (2007) find that when one considers stellar population age, rather than simply the colour bimodality, the morphology–density relation may be explained by an age–density relation and age–morphology relation (using more finely divided morphologies than our study). Their results imply that, in clusters, red spirals are younger than red early-types, and that both the morphology of a galaxy and its distance to the centre of the cluster are strongly related to the length of time since the galaxy’s star formation ceased, presumably when it entered the group environment. The timescale implied by red colour but visible spiral arms suggests that our red spirals are a likely candidate for the population of relatively-faint, red galaxies that has built up in clusters in recent times (Desai et al. 2007). Unless these red spirals are somehow ‘revived’, the only clear option for them is to evolve into galaxies resembling S0s. It is not a large step to presume that the objects that began their star-formation decline earliest may already appear to have S0 morphology. The existence of red spirals in dense environments thus lends support to the hypothesis of spirals evolving to S0s through environmental processes.

It seems likely that low mass S0s do form from spirals, while high mass S0s were formed more directly at an earlier

epoch, in a manner similar to ellipticals (Poggianti et al. 2001; Mehlert et al. 2003; Bedregal et al. 2008). However, Fig. 12 shows that a morphology–density relation exists at all stellar masses. Galaxies of all stellar masses are thus subject to environmental processes, though the mechanisms and the epoch at which they were effective may vary with mass. Candidate mechanisms, in order of declining effectiveness, include major mergers, minor mergers (Mihos & Hernquist 1994), harassment (Moore et al. 1996) and cluster tidal effects (Merritt 1983). All of these may heat or destroy a spiral’s stellar disk, leading to an early-type morphology. Our results clearly show that galaxy colour is transformed more readily than morphology, particularly for low mass galaxies, so we should expect to see significant numbers of red spirals, even if they will eventually evolve into S0s.

Figures 18 & 19 provide conclusive evidence for a process closely related to environment which causes galaxies with identical stellar mass and morphology to be more likely to be red in denser regions. This affects both spiral and early-type galaxies, though red spirals are more common than blue early-types. It affects low mass galaxies significantly more than those with high stellar mass. This process, or another, also results in an increase in the early-type fraction in dense environments, but a transition from blue to red is not generally accompanied by a transition from spiral to early-type. This rules out major mergers as the responsible mechanism, as they generally result in an early-type morphology (however, see Hopkins et al. (2008)). The most likely culprit is starvation (Larson et al. 1980), where the gaseous halo of a galaxy is removed by some environmental process, and therefore ceases to supply cold gas in the disk. As the current store is consumed by star formation, there is no more gas available and star formation declines and eventually terminates. The main candidate mechanisms for removing the halo gas are thermal evaporation (Cowie & Songaila 1977), ram-pressure stripping (Gunn & Gott 1972), viscous stripping (Nulsen 1982), and interaction with the cluster tidal field (Merritt 1983). Direct stripping of gas from the disks of galaxies may also be important within groups (Boselli & Gavazzi 2006). Note that at higher redshift, Poggianti et al. (2008) present signs that the environmental dependences of star formation and morphology may be more strongly linked than they are today. They also find an indication that star formation is enhanced in intermediate-density environments at $z \sim 0.6$ (see also Bamford et al. 2005), in contrast to the independence (e.g., Balogh et al. 2004) or suppression (e.g., Koopmann & Kenney 2004) of star formation with respect to increasing local density seen nowadays. This suggests that the dominant mechanism transforming galaxies in dense environments may change with cosmic time.

The cessation of star formation in galaxies entering the halo of a larger galaxy is a key ingredient of models of galaxy evolution, both semi-analytic models (e.g. Kauffmann et al. 1993) and analytic halo models (Cooray & Sheth 2002; Skibba & Sheth 2008). All of these models make a critical distinction between the central and satellite galaxies in a halo. The termination of star formation in satellites, and the manner in which it has been achieved, has generally been handled very simplistically in these models. Even so, with the addition of various assumptions, these models have met with considerable success in reproducing broad features of the galaxy population. Recent refinements have led to significant improvements in the quantitative agreement of model satellite colours with observations (Font et al. 2008; Skibba 2008). However, there are many aspects which remain to be reconciled with observations. In particular, comparison between the morphology dependences predicted by these models and observations has barely begun. The

dependence of morphology and colour on environment and stellar mass outlined in this paper provide clear observations with which to refine the next generation of models.

5 CONCLUSIONS

The Galaxy Zoo project has produced a catalogue of visual morphological galaxy classifications more than an order of magnitude larger than any previous catalogue. We have illustrated the biases present in this dataset, which are likely to have affected all previous work using morphologies to some extent, but which are only directly quantifiable in a dataset of this size. More importantly, we have demonstrated a procedure for measuring and correcting for these biases, such that they may be reliably used for statistical studies of morphological type fractions. Without this correction procedure the number of galaxies which may be used for such analyses is severely limited.

With the de-biased Galaxy Zoo dataset we have examined the relationship between morphological type fractions and environment, characterised by both local galaxy density and the distance to the nearest galaxy group. We reproduce the trends seen by earlier studies, but in much greater detail. The early-type fraction rises smoothly with increasing local density or decreasing groupcentric distance. Part of this trend is due to an increased proportion of massive galaxies in dense environments, which are preferentially early-types in any environment. However, at fixed stellar mass, a morphology–density relation is still present, with a similar change in early-type fraction with environment at all stellar masses.

Remarkably, the morphological fraction of group members varies very little with the mass of the group, either determined from the velocity dispersion or using integrated light as a mass proxy.

In studies based on modern surveys, galaxies on either side of the colour bimodality are often discussed in morphological language. However, colour and morphological fractions depend differently on environment. The fraction of red galaxies varies more strongly than the early-type fraction does. The result is that there is a considerably higher fraction of galaxies with red colour but spiral morphology in denser environments. There is also a substantial population of galaxies with blue colour but early-type morphology in low-density environments. The prevalence of red spirals peaks at intermediate local densities and within a few times the virial radius of galaxy groups. These objects mostly have true spiral morphology, and are additional to the S0 population. Their fraction decreases in the group cores and at the highest densities, although this is largely due to the rapidly declining fraction of all spirals in these regions. The fraction of spirals that are red increases steadily with density. Likewise, the fraction of early-types with blue colours declines steadily with increasing environmental density. High stellar mass galaxies, both spiral and early-type, are significantly less affected by their environment than galaxies with low stellar mass. Most low mass galaxies, of any morphology, are blue in the field and red in dense environments.

Only a small fraction of the colour–density relation is a consequence of the morphology–density relation. It is primarily driven by the environmental dependence of the fraction of red galaxies at fixed morphology: red spirals and blue early-types. Note that we consider morphology in terms of spiral versus early-type in this paper. It remains possible that there is a stronger link between the colour–density and morphology–density relations in terms of an environmental trend of morphology within the spiral class (i.e., Sa, Sb, Sc, ...). However, such a trend must be due to more gentle pro-

cesses than those which effect a full transformation from spiral to early-type. We therefore rule out mechanisms sufficiently violent to destroy galaxy disks, such as major mergers, as the primary cause of the colour-density relation.

These results catalogue a complex relationship between the morphology, colour, stellar mass and environment of galaxies, which successful models of galaxy formation and evolution must explain.

ACKNOWLEDGEMENTS

We are grateful to Ian Smail and David Wake for constructive comments on an earlier draft of this paper, and thank Ramin Skibba for insightful discussions. We also thank the referee for helpful comments which have improved the clarity of this paper.

This work has depended on the participation of many members of the public in visually classifying SDSS galaxies on the Galaxy Zoo website. We thank them for these extraordinary efforts in making this project a success. We are also indebted to various members of the media, both traditional and online, for helping to bring this project to the public's attention.

SPB acknowledges support from STFC. KL was funded by a Glasstone research fellowship, and further supported by Christ Church, Oxford. CJL acknowledges support from the STFC Science in Society Program. KS was supported by the Henry Skynner Junior Research Fellowship at Balliol College, Oxford.

Funding for the Sloan Digital Sky Survey (SDSS) and SDSS-II has been provided by the Alfred P. Sloan Foundation, the Participating Institutions, the National Science Foundation, the U.S. Department of Energy, the National Aeronautics and Space Administration, the Japanese Monbukagakusho, and the Max Planck Society, and the Higher Education Funding Council for England. The SDSS Web site is <http://www.sdss.org/>.

The SDSS is managed by the Astrophysical Research Consortium (ARC) for the Participating Institutions. The Participating Institutions are the American Museum of Natural History, Astrophysical Institute Potsdam, University of Basel, University of Cambridge, Case Western Reserve University, The University of Chicago, Drexel University, Fermilab, the Institute for Advanced Study, the Japan Participation Group, The Johns Hopkins University, the Joint Institute for Nuclear Astrophysics, the Kavli Institute for Particle Astrophysics and Cosmology, the Korean Scientist Group, the Chinese Academy of Sciences (LAMOST), Los Alamos National Laboratory, the Max-Planck-Institute for Astronomy (MPIA), the Max-Planck-Institute for Astrophysics (MPA), New Mexico State University, Ohio State University, University of Pittsburgh, University of Portsmouth, Princeton University, the United States Naval Observatory, and the University of Washington.

This paper has been typeset from a $\text{\TeX}/\text{\LaTeX}$ file prepared by the author.

REFERENCES

- Adelman-McCarthy J. K., et al., 2008, *ApJS*, 175, 297
 Allen P. D., Driver S. P., Graham A. W., Cameron E., Liske J., de Propris R., 2006, *MNRAS*, 371, 2
 Ann H. B., Park C., Choi Y.-Y., 2008, *MNRAS*, 389, 86

- Aragón-Salamanca A., Bedregal A. G., Merrifield M. R., 2006, *A&A*, 458, 101
 Baldry I. K., Balogh M. L., Bower R., Glazebrook K., Nichol R. C., 2004, in Allen R. E., Nanopoulos D. V., Pope C. N., eds, *The New Cosmology: Conference on Strings and Cosmology Vol. 743 of Am. Inst. of Phys. Conf. Series, Color bimodality: Implications for galaxy evolution*. pp 106–119
 Baldry I. K., Balogh M. L., Bower R. G., Glazebrook K., Nichol R. C., Bamford S. P., Budavari T., 2006, *MNRAS*, 373, 469
 Ball N. M., Loveday J., Brunner R. J., 2008, *MNRAS*, 383, 907
 Ball N. M., Loveday J., Fukugita M., Nakamura O., Okamura S., Brinkmann J., Brunner R. J., 2004, *MNRAS*, 348, 1038
 Balogh M., et al., 2004, *MNRAS*, 348, 1355
 Balogh M. L., Christlein D., Zabludoff A. I., Zaritsky D., 2001, *ApJ*, 557, 117
 Bamford S. P., Milvang-Jensen B., Aragón-Salamanca A., Simard L., 2005, *MNRAS*, 361, 109
 Barr J. M., Bedregal A. G., Aragón-Salamanca A., Merrifield M. R., Bamford S. P., 2007, *A&A*, 470, 173
 Bedregal A. G., Aragón-Salamanca A., Merrifield M. R., 2006, *MNRAS*, 373, 1125
 Bedregal A. G., Aragón-Salamanca A., Merrifield M. R., Cardiel N., 2008, *MNRAS*, 387, 660
 Biviano A., Murante G., Borgani S., Diaferio A., Dolag K., Girardi M., 2006, *A&A*, 456, 23
 Blakeslee J. P., et al., 2006, *ApJ*, 644, 30
 Blanton M. R., Berlind A. A., 2007, *ApJ*, 664, 791
 Blanton M. R., Eisenstein D., Hogg D. W., Schlegel D. J., Brinkmann J., 2005, *ApJ*, 629, 143
 Blanton M. R., et al., 2003a, *ApJ*, 594, 186
 Blanton M. R., et al., 2003b, *ApJ*, 592, 819
 Blanton M. R., Roweis S., 2007, *AJ*, 133, 734
 Boselli A., Gavazzi G., 2006, *PASP*, 118, 517
 Bower R. G., Benson A. J., Malbon R., Helly J. C., Frenk C. S., Baugh C. M., Cole S., Lacey C. G., 2006, *MNRAS*, 370, 645
 Burstein D., 1979, *ApJ*, 234, 435
 Butcher H., Oemler Jr. A., 1984, *ApJ*, 285, 426
 Cameron E., Driver S. P., 2007, *MNRAS*, 377, 523
 Ceccarelli L., Padilla N., Lambas D. G., 2008, *MNRAS*, 390, L9
 Christlein D., Zabludoff A. I., 2004, *ApJ*, 616, 192
 Conselice C. J., 2003, *ApJS*, 147, 1
 Conselice C. J., 2006, *MNRAS*, 373, 1389
 Cooray A., Sheth R., 2002, *Phys. Rep.*, 372, 1
 Couch W. J., Barger A. J., Smail I., Ellis R. S., Sharples R. M., 1998, *ApJ*, 497, 188
 Cowie L. L., Songaila A., 1977, *Nature*, 266, 501
 Croton D. J., et al., 2005, *MNRAS*, 356, 1155
 Croton D. J., et al., 2006, *MNRAS*, 365, 11
 Croton D. J., Farrar G. R., 2008, *MNRAS*, 386, 2285
 de Jong R., 1995, PhD thesis, PhD thesis. Univ. Groningen
 Desai V., et al., 2007, *ApJ*, 660, 1151
 Dressler A., 1980a, *ApJS*, 42, 565
 Dressler A., 1980b, *ApJ*, 236, 351
 Dressler A., et al., 1997, *ApJ*, 490, 577
 Dressler A., Gunn J. E., 1992, *ApJS*, 78, 1
 Faber S. M., et al., 2007, *ApJ*, 665, 265
 Fan L., Lapi A., De Zotti G., Danese L., 2008, *ArXiv e-prints*
 Font A. S., et al., 2008, *MNRAS*, 389, 1619
 Fukugita M., et al., 2007, *AJ*, 134, 579
 Gallazzi A., Charlot S., Brinchmann J., White S. D. M., Tremonti C. A., 2005, *MNRAS*, 362, 41

- Gavazzi G., Franzetti P., Scodreggio M., Boselli A., Pierini D., 2000, *A&A*, 361, 863
- Gisler G. R., 1980, *AJ*, 85, 623
- Glazebrook K., et al., 2004, *Nature*, 430, 181
- Gómez P. L., et al., 2003, *ApJ*, 584, 210
- Goto T., et al., 2003, *PASJ*, 55, 757
- Goto T., Yamauchi C., Fujita Y., Okamura S., Sekiguchi M., Smail I., Bernardi M., Gomez P. L., 2003, *MNRAS*, 346, 601
- Gunn J. E., Gott J. R. I., 1972, *ApJ*, 176, 1
- Haines C. P., Gargiulo A., La Barbera F., Mercurio A., Merluzzi P., Busarello G., 2007, *MNRAS*, 381, 7
- Haines C. P., La Barbera F., Mercurio A., Merluzzi P., Busarello G., 2006, *ApJ*, 647, L21
- Hogg D. W., et al., 2004, *ApJ*, 601, L29
- Hopkins P. F., Cox T. J., Younger J. D., Hernquist L., 2008, *ArXiv e-prints*
- Hubble E., Humason M. L., 1931, *ApJ*, 74, 43
- Hubble E. P., 1922, *ApJ*, 56, 162
- Huchra J., Davis M., Latham D., Tonry J., 1983, *ApJS*, 52, 89
- Huchra J. P., Geller M. J., 1982, *ApJ*, 257, 423
- James P. A., Knapen J. H., Shane N. S., Baldry I. K., de Jong R. S., 2008, *A&A*, 482, 507
- Jones L. R., Ponman T. J., Horton A., Babul A., Ebeling H., Burke D. J., 2003, *MNRAS*, 343, 627
- Kaiser N., 1987, *MNRAS*, 227, 1
- Kauffmann G., et al., 2003, *MNRAS*, 341, 33
- Kauffmann G., White S. D. M., Guiderdoni B., 1993, *MNRAS*, 264, 201
- Kauffmann G., White S. D. M., Heckman T. M., Ménard B., Brinchmann J., Charlot S., Tremonti C., Brinkmann J., 2004, *MNRAS*, 353, 713
- Koopmann R. A., Kenney J. D. P., 2004, *ApJ*, 613, 866
- Lahav O., et al., 1995, *Science*, 267, 859
- Land K., et al., 2008, *MNRAS*, 388, 1686
- Lane K. P., Gray M. E., Aragón-Salamanca A., Wolf C., Meisenheimer K., 2007, *MNRAS*, 378, 716
- Larson R. B., Tinsley B. M., Caldwell C. N., 1980, *ApJ*, 237, 692
- Lewis I., et al., 2002, *MNRAS*, 334, 673
- Lin Y.-T., Mohr J. J., Gonzalez A. H., Stanford S. A., 2006, *ApJ*, 650, L99
- Lintott C. J., et al., 2008, *MNRAS*, 389, 1179
- Lupton R., Blanton M. R., Fekete G., Hogg D. W., O'Mullane W., Szalay A., Wherry N., 2004, *PASP*, 116, 133
- Maller A. H., 2008, *ArXiv: 0801.4568*, 801
- Maller A. H., Berlind A. A., Blanton M. R., Hogg D. W., 2008, *ArXiv: 0801.3286*, 801
- Mehlert D., Thomas D., Saglia R. P., Bender R., Wegner G., 2003, *A&A*, 407, 423
- Merritt D., 1983, *ApJ*, 264, 24
- Mihos J. C., Hernquist L., 1994, *ApJ*, 425, L13
- Miller C. J., et al., 2005, *AJ*, 130, 968
- Mo H. J., White S. D. M., 2002, *MNRAS*, 336, 112
- Mo H. J., Yang X., van den Bosch F. C., Jing Y. P., 2004, *MNRAS*, 349, 205
- Moore B., Katz N., Lake G., Dressler A., Oemler A., 1996, *Nature*, 379, 613
- Nakamura O., Fukugita M., Brinkmann J., Schneider D. P., 2004, *AJ*, 127, 2511
- Nulsen P. E. J., 1982, *MNRAS*, 198, 1007
- Padmanabhan N., et al., 2008, *ApJ*, 674, 1217
- Park C., Choi Y.-Y., Vogeley M. S., Gott J. R. I., Blanton M. R., 2007, *ApJ*, 658, 898
- Pimblet K. A., Smail I., Kodama T., Couch W. J., Edge A. C., Zabludoff A. I., O'Hely E., 2002, *MNRAS*, 331, 333
- Poggianti B. M., et al., 2001, *ApJ*, 563, 118
- Poggianti B. M., et al., 2006, *ApJ*, 642, 188
- Poggianti B. M., et al., 2008, *ApJ*, 684, 888
- Poggianti B. M., Smail I., Dressler A., Couch W. J., Barger A. J., Butcher H., Ellis R. S., Oemler A. J., 1999, *ApJ*, 518, 576
- Postman M., et al., 2005, *ApJ*, 623, 721
- Postman M., Geller M. J., 1984, *ApJ*, 281, 95
- Rojas R. R., Vogeley M. S., Hoyle F., Brinkmann J., 2004, *ApJ*, 617, 50
- Rojas R. R., Vogeley M. S., Hoyle F., Brinkmann J., 2005, *ApJ*, 624, 571
- Schawinski K., et al., 2007, *ApJS*, 173, 512
- Schawinski K., et al., 2008, submitted to *MNRAS*
- Schawinski K., Thomas D., Sarzi M., Maraston C., Kaviraj S., Joo S.-J., Yi S. K., Silk J., 2007, *MNRAS*, 382, 1415
- Sheth R. K., Tormen G., 1999, *MNRAS*, 308, 119
- Simard L., et al., 2002, *ApJS*, 142, 1
- Skibba R., Sheth R. K., Connolly A. J., Scranton R., 2006, *MNRAS*, 369, 68
- Skibba R. A., 2008, *ArXiv: 0805.1233*, 805
- Skibba R. A., Sheth R. K., 2008, *ArXiv e-prints*
- Slosar A., et al., 2008, submitted to *MNRAS*
- Smail I., Dressler A., Couch W. J., Ellis R. S., Oemler A. J., Butcher H., Sharples R. M., 1997, *ApJS*, 110, 213
- Smith G. P., Treu T., Ellis R. S., Moran S. M., Dressler A., 2005, *ApJ*, 620, 78
- Stoughton C., et al., 2002, *AJ*, 123, 485
- Strauss M. A., et al., 2002, *AJ*, 124, 1810
- Torki M., et al., 2008, submitted to *MNRAS*
- Treu T., Ellis R. S., Kneib J.-P., Dressler A., Smail I., Czoske O., Oemler A., Natarajan P., 2003, *ApJ*, 591, 53
- van den Bergh S., 1976, *ApJ*, 206, 883
- van den Bergh S., 2007, *AJ*, 134, 1508
- van den Bosch F. C., Pasquali A., Yang X., Mo H. J., Weinmann S., McIntosh D. H., Aquino D., 2008, *ArXiv: 0805.0002*, 805
- van der Wel A., 2008, *ApJ*, 675, L13
- van der Wel A., et al., 2007, *ApJ*, 670, 206
- Vogt N. P., Haynes M. P., Giovanelli R., Herter T., 2004, *AJ*, 127, 3300
- von der Linden A., Best P. N., Kauffmann G., White S. D. M., 2007, *MNRAS*, 379, 867
- Wake D. A., et al., 2006, *MNRAS*, 372, 537
- Weinmann S. M., van den Bosch F. C., Yang X., Mo H. J., 2006, *MNRAS*, 366, 2
- Whitmore B. C., Gilmore D. M., 1991, *ApJ*, 367, 64
- Whitmore B. C., Gilmore D. M., Jones C., 1993, *ApJ*, 407, 489
- Wolf C., et al., 2007, Vol. 211 of *AAS Meeting Abstracts, Optically Passive Infall Spirals In Stages: Star Formation Only Semi-quenched*. p. 67.01
- Wolf C., et al., 2008, submitted to *MNRAS*
- Wolf C., Gray M. E., Aragón-Salamanca A., Lane K. P., Meisenheimer K., 2007, *MNRAS*, 376, L1
- Yamauchi C., Goto T., 2004, *MNRAS*, 352, 815
- Yoon J. H., Schawinski K., Sheen Y.-K., Ree C. H., Yi S. K., 2008, *ApJS*, 176, 414
- Zehavi I., et al., 2002, *ApJ*, 571, 172

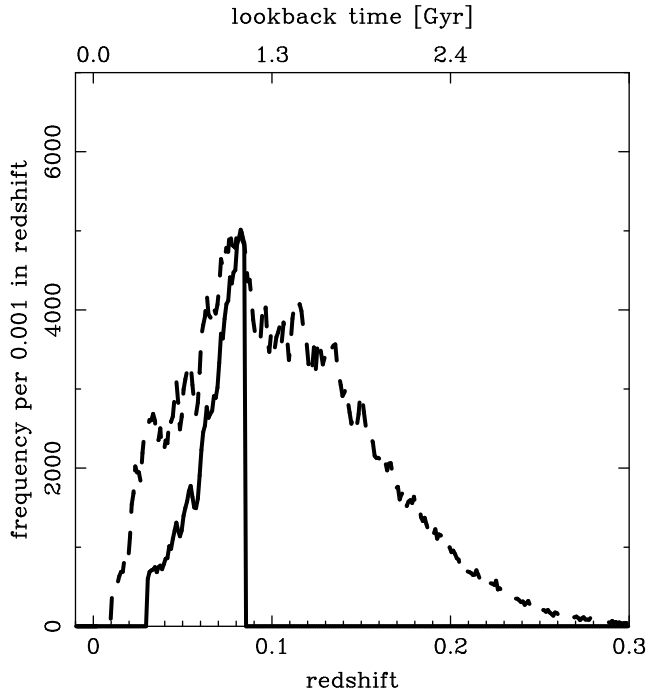


Figure A1. The redshift distribution of the *luminosity-limited sample* analysed in this paper (solid line) and the SDSS Main Galaxy Sample (dashed line) from which it is drawn.

APPENDIX A: QUANTIFYING CLASSIFICATION BIAS

A1 Demonstrating the bias

In the absence of evolution in the galaxy population, the true distribution of galaxy morphologies does not change with redshift. However, the apparent brightness and size of a given galaxy depends on the distance at which it is viewed, and so its measured morphology may vary with redshift. We term this *classification bias*.

For example, a spiral galaxy viewed nearby may be easy to classify correctly, but if viewed at higher redshift the lower signal-to-noise and smaller size, relative to the atmospheric seeing, would make the same galaxy appear as a ‘fuzzy blob’. Classifiers with a good understanding of these issues will tend to recognise these limitations and assign such an object to the unclassified category, though not always. Non-experts, such as the vast majority of Galaxy Zoo participants, will more frequently classify such an object as an early-type. This is exacerbated by the scaling of images to always present objects at a similar size on-screen, as was done for Galaxy Zoo. However, it is likely that all morphological studies are affected by classification bias to some extent, even including those studies performed by expert classifiers with the ability to vary the characteristics of the image display. This is the first study with a sample of morphologically classified objects that is sufficiently large for this bias to be directly quantified.

The redshift range probed by the majority of our Galaxy Zoo *full sample*, $0.03 \lesssim z \lesssim 0.15$, (see Fig. A1) corresponds to an interval of 1.5 Gyr. This is 10 per cent of the age of the universe, during its most quiescent period. Over this period the galaxy population has not changed greatly. The latest studies of evolution in the luminosity functions of red and blue galaxies find a ~ 2 increase in the ratio of red versus blue galaxies since $z \sim 1$ (Faber et al. 2007), which roughly corresponds to ~ 30 per cent over the redshift range of the Galaxy Zoo sample. However, this figure is fairly uncertain

as it is not clear when during the $z = 0 - 1$ period most of this evolution occurred. In demonstrating and quantifying classification bias in the Galaxy Zoo data we will often assume negligible evolution. If this assumption is not valid, then the classification bias we measure will also include a contribution due to galaxy evolution. Ultimately, our aim for this paper is to correct the raw Galaxy Zoo classifications so that objects over the range of redshifts sampled may be combined. Removing any evolution, in addition to classification bias, will help us to achieve this aim.

Observational limitations can introduce a variation in the population of galaxies that is sampled at different redshifts. Quantities measured from the sample may therefore vary with redshift, even if the galaxy population does not. This is termed *selection bias*. For example, intrinsically faint objects can only be detected nearby, while luminous objects are rare and so only appear in the sample at larger distances where the sampled volume is larger. The apparent magnitude limit and volume effect dominate the variation in sample selection with redshift. Figure 1 (in the main part of the paper) indicates that redshift-dependent biases are present in the GZ data, but does not discriminate between classification and selection biases. However, by considering objects in narrow bins of intrinsic luminosity, i.e. absolute magnitude, we can remove the effects of this component of selection bias.

Figure A2 illustrates the variation in morphological type fraction as a function of redshift for galaxies in three absolute magnitude intervals. If evolution is negligible, there are no selection biases with respect to quantities other than apparent magnitude, and in the absence of classification bias, we would expect these type fractions to be constant with redshift. Note that the fractions change between different absolute magnitude bins due to selection effects and the inherent correlation between morphology and luminosity.

Intrinsically bright objects are included in the Galaxy Zoo selection limits over a fairly wide redshift range. Their type fractions remain fairly constant with redshift, as expected if there is no classification bias. However, the majority of objects with this luminosity are truly early-types, and hence free from the classification bias effect. The primary trend is a gradual increase in the fraction of galaxies classified as ‘don’t know’, mostly at the expense of spirals.

At more typical galaxy luminosities and fainter, a gradient in the type fractions versus redshift is obvious. Towards higher redshifts a greater fraction of objects are classified as early-type rather than spiral. A strong classification bias therefore appears to be present in the data, with apparently faint galaxies being preferentially classified as early-type, presumably because fewer details may be discerned given the noise. The presence of classification bias is also indicated by the thin lines in Fig. 2 (in the main part of the paper), which shows type fraction trends based on the raw type likelihoods with selection effects removed below a given redshift by imposing a faint magnitude limit.

In Fig. A2, the turn-up in the spiral fraction at the highest redshifts probed in each luminosity bin is a reversal of the more general bias, and its origin is unclear. Plausible possibilities affecting the faintest galaxies are that the users realise they are seeing a blurred image and attempt to compensate with their classifications, that noise artifacts are more frequently interpreted as structure, or that early-types are being lost as a result of the effective size selection limit. However, it does not appear to be a significant effect for the redshift ranges considered in the main part of this paper.

In addition to apparent magnitude, the other main factor influencing a Galaxy Zoo classifier’s ability to accurately determine a galaxy’s morphological type is its apparent size. However, if

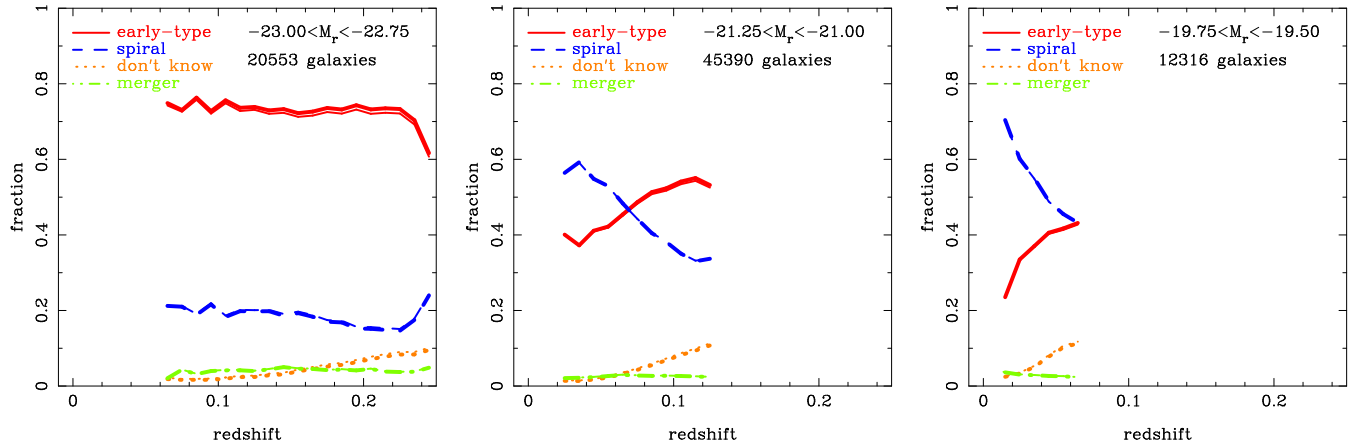


Figure A2. Morphological type fraction versus redshift for galaxies in three example bins of absolute magnitude from our *full sample*. The thick and thin lines corresponds to the weighted and unweighted samples, respectively.

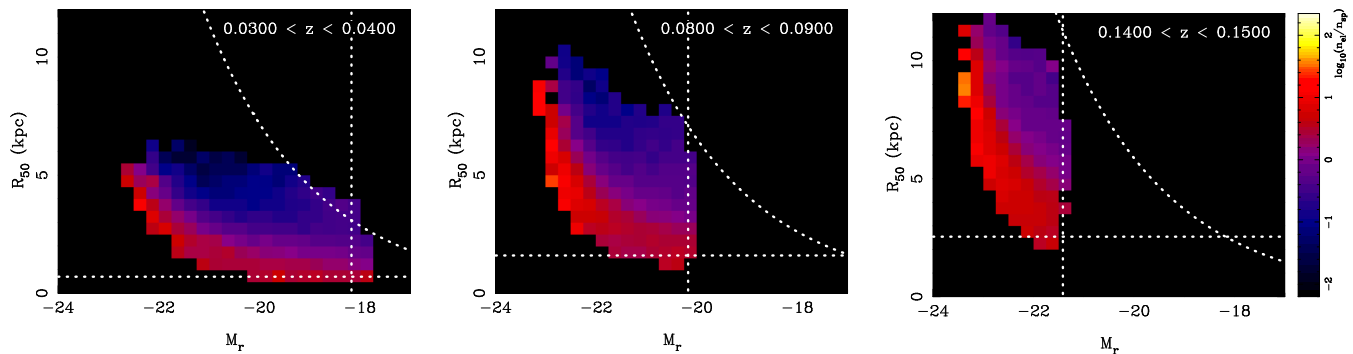


Figure A3. Ratio of the early-type to spiral measured type likelihoods as a function of absolute magnitude and physical size, for galaxies in three example redshift bins. The logarithmic colour scale is shown by the bar on the right. The dotted lines indicate the $r = 17.77$ apparent magnitude limit, $\mu_{50,r} = 23$ mag arcsec $^{-2}$ apparent surface brightness limit, and the physical scale corresponding to an angle of 1 arcsec, at the central redshift of each bin.

we consider the measured type fractions versus redshift in bins of physical size (in kpc), then the apparent magnitude selection effects are not accounted for and dominate, together with the intrinsic correlation between luminosity and size (e.g. de Jong 1995; Cameron & Driver 2007).

We therefore need to consider the measured type fractions as a bivariate function of both luminosity and size¹. In this paper we are concerned with the early-type and spiral fractions. Studying the merger candidates will be an interesting topic for future studies, but their classification is complicated by additional biases. In any case the numbers of objects classified as mergers are low. The ‘don’t know’ option provides an indication of where the classifiers themselves feel they are unable to determine accurate classifications. This supplies supplementary information for judging the unbiased region of parameter space, but ideally we wish to determine this directly from the biases in the measured type likelihoods. We therefore concentrate on the ratio of early-type to spiral likelihoods for the remainder of this paper. This ratio is plotted for three example redshift bins in Fig. A3. The number of galaxies in each luminosity–size–redshift bin are shown in Fig. A4.

Assuming evolution is negligible, and that any selection biases are functions of only apparent magnitude and size (including

surface brightness, which depends on both), then in the absence of classification bias, we would expect the ratio of early-types to spirals to be constant with redshift.

In simple terms, in Fig. A3 changes in the colour (type ratio) of a particular square (luminosity–size bin) between redshift slices indicate a redshift dependent classification bias. This bias is due to the decreasing signal-to-noise and resolution for similar galaxies viewed at increasing redshifts. A movie is available in the online supplementary material, which steps through this plot in redshift slices and demonstrates the effect more clearly.

A2 Constructing a baseline correction

To quantify how classification bias changes with redshift, as a function of luminosity and size, we first construct an estimate of the n_{el}/n_{sp} versus luminosity and size in the absence of any redshift-dependent classification bias. To do this, for each luminosity–size bin we find the lowest redshift bin that contains at least a certain number of galaxies, and assume that the ratio in this bin is accurate. We take the minimum number of galaxies required in a bin to be 30.

From inspecting Fig. A3 this approach appears to be reasonable. At low redshift the *full sample* includes faint, small galaxies. Those well inside the apparent magnitude, size and surface brightness limits should be unbiased. At higher redshifts, these limits become more restrictive, and biases grow at the faint, small end of the

¹ We could have chosen to use surface brightness in place of either luminosity or size, but we find that surface brightness alone is not sufficient to describe the behaviour of the bias.

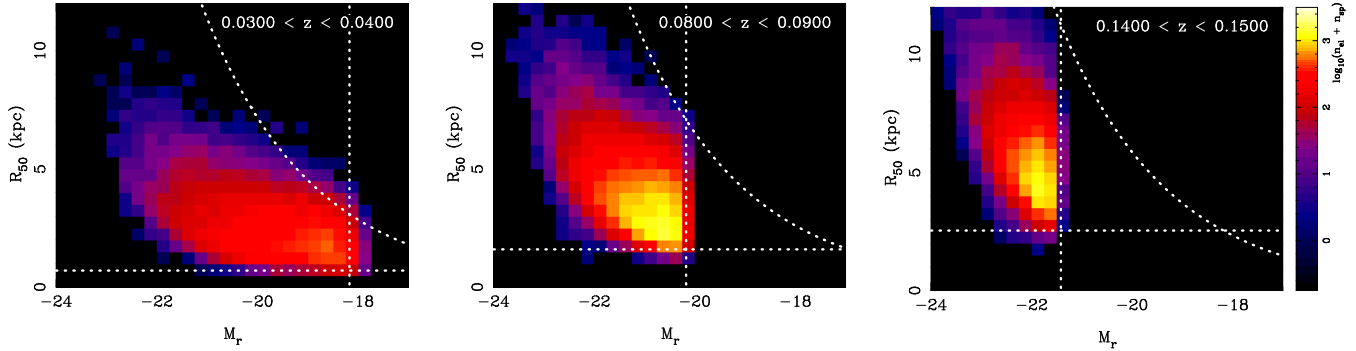


Figure A4. Number of early-type and spiral galaxies in each bin of absolute magnitude and physical size, for three example redshift bins. The logarithmic colour scale is shown on the right. Dotted lines are as in Fig. A3.

galaxy distribution. The scarcity of bright, large galaxies means that they are only seen in significant numbers at higher redshifts, where the survey encompasses a larger volume. However, at the redshifts at which n_{el}/n_{sp} can be estimated for these galaxies, they are still well within the luminosity and size limits, helped by the intrinsic size–luminosity relation. On the other hand, the surface brightness limit may cause residual biases for the largest galaxies at a given luminosity. In order to avoid these biases, we further restrict the bins considered to those which are 1 mag arcsec $^{-1}$ brighter than the surface brightness limit, 1 mag brighter than the magnitude limit, and with size greater than twice the angular resolution at each redshift. The resulting plot should be unbiased, or as close as can be reasonably achieved given the available data.

Taking this approach we obtain a baseline estimate of the unbiased early-type to spiral ratio versus luminosity and size at $z \sim 0$, shown in Fig. A5. This figure clearly shows a region of luminosity–size space dominated by early-types (lower-left) and another dominated by spirals (upper-right), with a fairly sharp, curved transition between the two. There are a small number of galaxies in the *Galaxy Zoo full sample* which are located in an area of luminosity–size space for which we do not have a direct estimate of the local early-type to spiral ratio, due to a combination of the low numbers of objects in these areas and their excision to avoid including potentially biased regions in the baseline estimate. In order to extrapolate to these regions, as well as generally removing noise and reducing the impact of residual bias, it is advantageous to fit a smooth function to the binned baseline estimate.

Motivated by the observed behaviour of the early-type to spiral ratio versus luminosity and size, after trying a variety of functions we choose the following to fit the local baseline estimate:

$$\frac{n_{el}}{n_{sp}} = \frac{p_1}{1 + \exp\left(\frac{s_1(R_{50}) - M_r}{s_2(R_{50})}\right)} + p_2, \quad (\text{A1})$$

This gives a smooth step function in M_r with position and width varying with R_{50} as

$$s_1(R_{50}) = q_1^{-(q_2 + q_3 R_{50}^{q_4})} + q_5, \quad (\text{A2})$$

and

$$s_2(R_{50}) = r_1 + r_2(s_1(R_{50}) - q_5),$$

respectively.

This fit, shown in Fig. A6, provides a smooth local baseline estimate against which we can compare the raw early-type to spiral ratio versus luminosity and size as a function of redshift. In this manner we can derive a correction that will remove the majority of the classification bias, including all of its redshift dependence over our

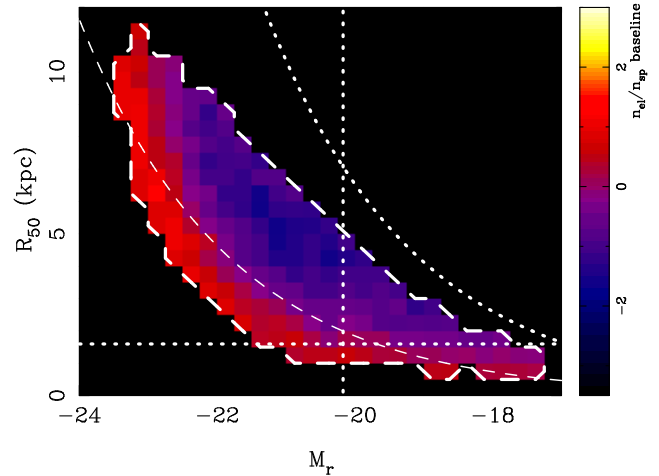


Figure A5. Baseline estimate of the local unbiased early-type to spiral ratio versus luminosity and size. The dotted lines indicate the $r = 17.77$ apparent magnitude limit, $\mu_{50,r} = 23$ mag arcsec $^{-2}$ apparent surface brightness limit, and the physical scale corresponding to an angle of 1 arcsec, at the $z = 0.085$ upper redshift limit of the analysis samples (see Sec. 2.1). The thin dashed curve indicates an apparent surface brightness of $\mu_{50,r} = 20.25$ mag arcsec $^{-2}$. This approximately separates early-types and spirals, but clearly a simple surface brightness dependence is not sufficient to describe all the behaviour in this plot.

sample. This method will also remove any evolution effects in this quantity, if present over the limited redshift range of the sample.

To estimate the correction, $C(M_r, R_{50}, z)$, we simply determine the difference between n_{el}/n_{sp} in each redshift bin and the baseline just determined. This correction is plotted for three example redshift bins in Fig. A7. The dependence of the correction on redshift is shown for a few example bins in Fig. A8.

At this point we have a baseline correction in bins of luminosity, size and redshift, $C(M_r, R_{50}, z)$. A small fraction of galaxies lie in regions of parameter space containing insufficient objects to determine a direct correction. For galaxies in these bins we use the mean correction for the nearest neighbours within 1.2 times the distance to the nearest bin centre. This has the advantage of averaging over bins when there are several at similar distances. This extrapolation is only valid close to the region which has a directly determined correction, but it only needs to be, as there are very few galaxies far from this region.

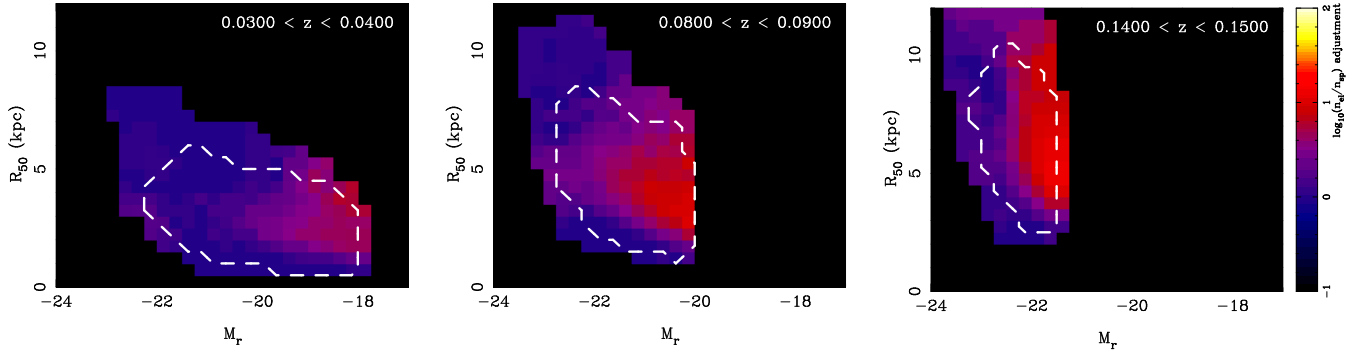


Figure A7. Difference between the raw $\log_{10}(n_{el}/n_{sp})$ in three example redshift bins and the baseline. This is the adjustment that must be applied to the value in each luminosity–size–redshift bin to remove the classification bias. The colour scale is shown by the bar on the right. The region enclosed by the dashed line is determined from the data, while outside this region the adjustment is estimated from the nearest well-determined bins. Only the region containing significant galaxy counts is coloured.

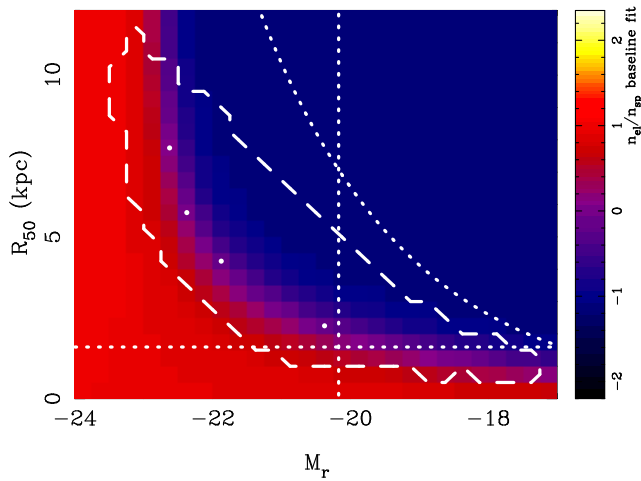


Figure A6. Fitted baseline estimate of the local unbiased early-type to spiral ratio versus luminosity and size. Dotted lines are as in Fig. A5. The four white dots indicate the bins plotted in Fig. A8.

A3 De-biased Galaxy Zoo samples

The baseline correction derived above can now be directly applied to de-bias the raw type likelihoods. To obtain the de-biased type likelihoods we adjust the raw likelihoods of each galaxy as

$$p_{el,adj} = \frac{1}{1/\left(\frac{p_{el}}{p_{sp}}\right)_{adj} + \frac{p_x}{p_{el}} + 1}, \quad (\text{A3})$$

$$p_{sp,adj} = \frac{1}{\left(\frac{p_{el}}{p_{sp}}\right)_{adj} + \frac{p_x}{p_{sp}} + 1},$$

where

$$\left(\frac{p_{el}}{p_{sp}}\right)_{adj} = \left(\frac{p_{el}}{p_{sp}}\right)_{raw} / 10^{C(M_r, R_{50}, z)} \quad (\text{A4})$$

and $p_x = 1 - p_{el} - p_{sp}$.

This effect of this adjustment is shown in Fig. A9. The overall effect is to lower the early-type likelihoods, particularly for objects where there is some indication that the object shows spiral features in the raw likelihood. The largest effect is for galaxies around the median redshift of our *full sample*. For lower redshifts most galaxies are well classified and need little adjustment. For higher redshifts only the most luminous objects are selected, the majority of

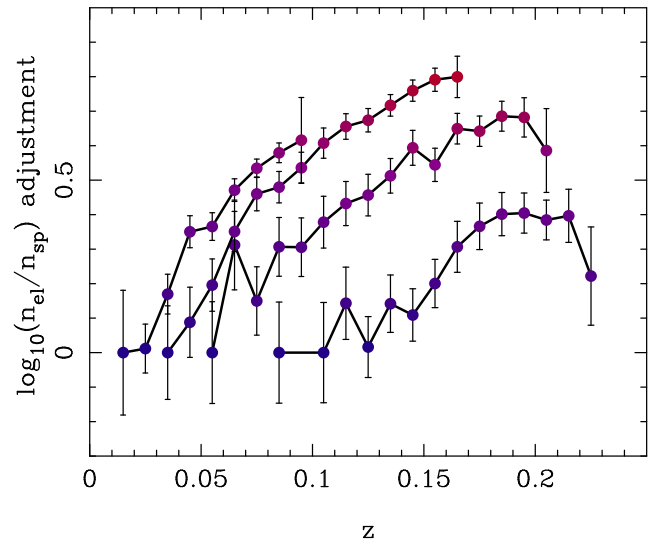


Figure A8. Redshift dependence of the correction to $\log_{10}(n_{el}/n_{sp})$ for a few example luminosity–size bins, at $(M_r, R_{50}) = (-22.625, 7.75), (-22.375, 5.75), (-21.875, 4.25), (-20.375, 2.25)$, as indicated by the white dots in Fig. A6. The colours of the points corresponds to the colour scale Fig. A7.

which are truly early-types and therefore do not suffer from the bias.

The success of our de-biasing procedure is demonstrated by Figs. 2 & 7 in the main body of this paper, which show that the method works as expected.

APPENDIX B: 'FINGERS OF GOD' CORRECTION

The high velocity dispersions in galaxy groups lead one to grossly overestimate the line-of-sight distances between the group centre and its member galaxies, when a cosmological conversion between redshift and distance is assumed. We correct for this effect by reducing the distance to the group centre for galaxies with redshifts consistent with the group redshift and velocity dispersion, and close to the group in projected distance. Specifically, we determine the line-of-sight comoving distance between the galaxy and group centre as

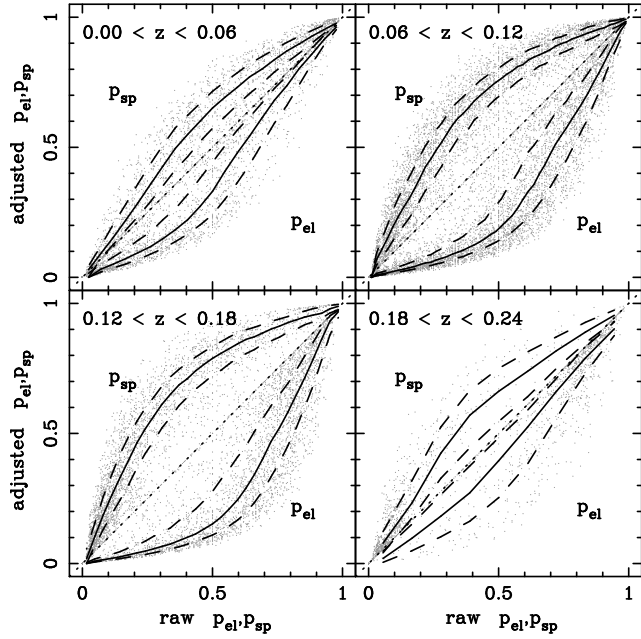


Figure A9. De-biased type likelihoods versus the raw values direct from the Galaxy Zoo classifications. The dotted diagonal line indicates the one-to-one relation. Points above and below this line refer to the spiral and early-type likelihoods, respectively. The solid and dashed lines trace the median and quartiles of the points.

$$d_{\text{los}} = d_c \left(1 - e^{-A(|z_{\text{gal}} - z_{\text{grp}}|/\zeta)^B} e^{-C(\max(R_{\text{vir}}, d_{\text{pro}}) - R_{\text{vir}})^D} \right), \quad (\text{B1})$$

where A , B , C and D are chosen to ensure the following behaviour. For galaxies with projected distances $\leq R_{\text{vir}}$: $d_{\text{los}} = 0$ when $z_{\text{gal}} = z_{\text{grp}}$; $d_{\text{los}} = R_{\text{vir}}$ when $|z_{\text{gal}} - z_{\text{grp}}| = \zeta$; and the adjustment is less than 1 per cent when $|z_{\text{gal}} - z_{\text{grp}}| \geq 2\zeta$. Here, $\zeta = 3\sigma_{\text{grp}}(1 + z_{\text{grp}})/c_0$ is the redshift difference corresponding to three times the group velocity dispersion, d_c is the comoving distance between the galaxy and group redshifts assuming only cosmological motions, and d_{pro} is the projected distance between the galaxy and the group's brightest member assuming they both lie at the group cosmological redshift. For galaxies with $d_{\text{pro}} > R_{\text{vir}}$ the adjustment is decreased to 90 per cent of its $\leq R_{\text{vir}}$ value by $d_{\text{pro}} = 2R_{\text{vir}}$ and 1 per cent of its $\leq R_{\text{vir}}$ value by $d_{\text{pro}} = 5R_{\text{vir}}$.

We furthermore normalise the corrected distances by R_{vir} of the nearest group to account for scaling of any potential influence with group size. Figure B1 illustrates the effect of the correction for model galaxies in a typical C4 group. A comparison of the redshift-space distances, $d_{C4} = \sqrt{d_c^2 + d_{\text{pro}}^2}$ and the normalised, corrected distances, $D_{C4} = \sqrt{d_{\text{los}}^2 + d_{\text{pro}}^2} / R_{\text{vir}}$, is shown in Fig. B2.

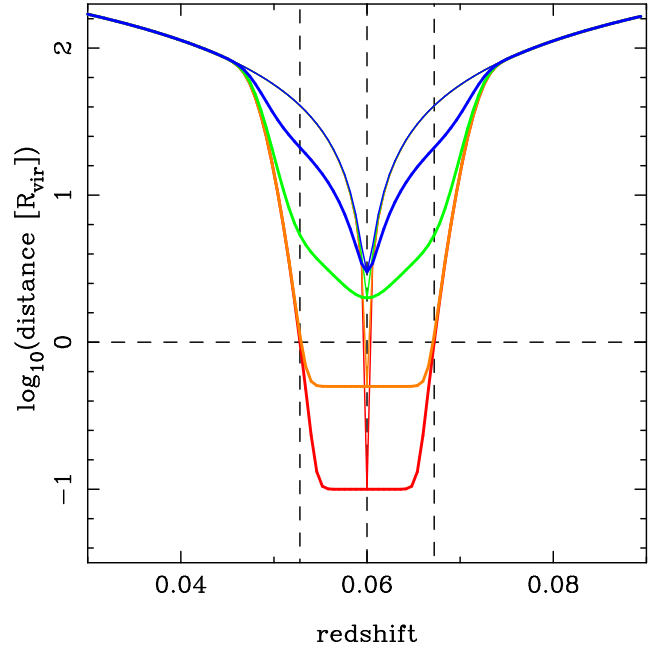


Figure B1. Illustration of the ‘Fingers of God’ suppression method. Coloured lines show the relation between redshift and the logarithmic distance, in virial radii, to a group with properties typical of those in the C4 catalogue: $z = 0.06$, $\sigma = 680 \text{ km s}^{-1}$ and $R_{\text{vir}} = 0.74 \text{ Mpc}$. Thin, solid lines plot the relation assuming no peculiar velocities. In this case, small departures from the cluster redshift imply large distances. However, in reality, peculiar velocities impart significant redshift differences on galaxies that are actually members of the group, and so at small distances from one another. Thick solid lines show the relation with the ‘Fingers of God’ suppression method, which attempts to account for this. The red, orange, green and blue lines indicate the effect on galaxies at projected separations of 0.1, 0.5, 2, and 3 R_{vir} , respectively.

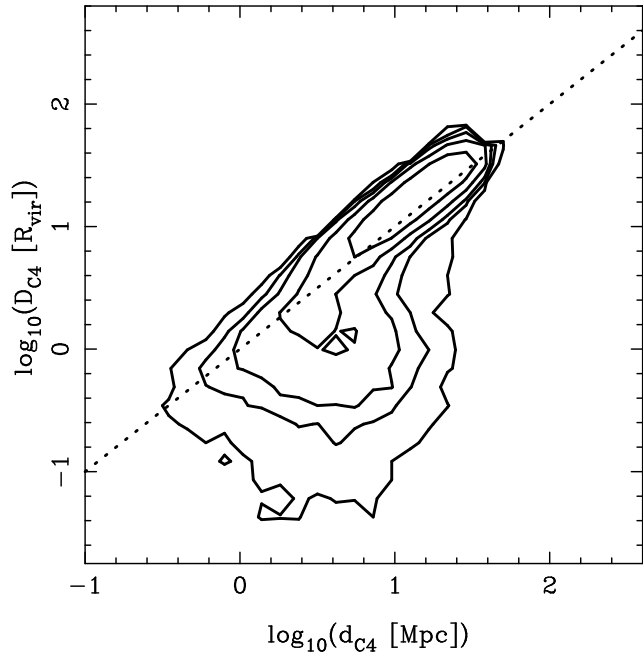


Figure B2. Redshift-space distance of each galaxy to its nearest C4 group, d_{C4} , versus a measure of this distance incorporating a correction for the 'Fingers of God' effect and normalised by virial radius, D_{C4} . Contours enclose 50, 75, 90, 95 and 99 per cent of galaxies in the *luminosity-limited sample*.